Journal Pre-proof

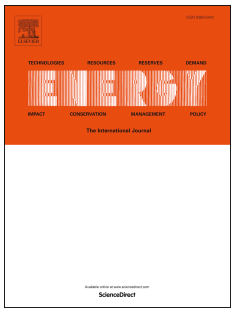

Optimization of a multi-generation power, desalination, refrigeration and heating system

Ariana M. Pietrasanta, Sergio F. Mussati, Pio A. Aguirre, Tatiana Morosuk, Miguel C. Mussati

PII: S0360-5442(21)01985-X

DOI: https://doi.org/10.1016/j.energy.2021.121737

Reference: EGY 121737

To appear in: *Energy*

Received Date: 9 March 2021

Revised Date: 25 July 2021

Accepted Date: 6 August 2021

Please cite this article as: Pietrasanta AM, Mussati SF, Aguirre PA, Morosuk T, Mussati MC, Optimization of a multi-generation power, desalination, refrigeration and heating system, *Energy*, https://doi.org/10.1016/j.energy.2021.121737.

Credit Author Statement:

Ariana Pietrasanta: Software; Investigation**. Sergio F. Mussati**: Methodology; Investigation; Writing- Original draft preparation. **Pio A. Aguirre**: Reviewing and Editing; **Tatiana Morosuk**: Reviewing and Editing. **Miguel C. Mussati**: Methodology; Writing- Reviewing and Editing; Supervision.

Optimization of a multi-generation power, desalination, refrigeration and heating system

Ariana M. Pietrasanta[1], Sergio F. Mussati[1], Pio A. Aguirre[1], Tatiana Morosuk[2], Miguel C. Mussati[1*]

[1] INGAR Instituto de Desarrollo y Diseño (CONICET-UTN), Avellaneda 3657, 3000, Santa Fe, Argentina

[2] Institute for Energy Engineering, Technishe Universität Berlin, Marchstrs. 18, Berlin, Germany

Abstract

The optimization of a multi-generation system which represents the integrated dual-purpose desalination plant and a low-scale absorption refrigeration system is addressed. A nonlinear mathematical programming optimization model that integrates a natural gas combined-cycle, a multi-effect distillation desalination plant, a series flow double-effect water-lithium bromide absorption refrigeration system, and a water heater, is developed based on first-principle models. The model is implemented in General Algebraic Modelling System and a generalized gradient-based optimization algorithm is used.

Given design specifications for electricity generation (around 37 MW), freshwater production (100 kg/s), refrigeration capacity (2 MW), and thermal load for heating (around 0.7 MW of hot water), the integrated system is optimized by minimizing two objective functions by single-objective optimization: total heat transfer area and total annual cost. As a result, minimum total heat transfer area values of 39148 m^2, 36002 m^2, and 35161 m^2 are obtained when 4, 5, and 6 distillation effects were considered in the multi-effect distillation system, respectively. Also, a minimum annual cost of around 24 MM$/yr. is obtained for 5 distillation effects.

The influence of the number of effects in the multi-effect distillation subsystem on the optimal solutions is analyzed. Cost-effective optimal solutions are developed for the studied multi-generation system.

***Keywords*:** Multi-generation; dual-purpose desalination; absorption refrigeration system; optimization; nonlinear programming NLP; GAMS

Nomenclature

Variable symbols

A	heat transfer area of a process unit (m^2)
annCAPEX	annualized capital expenditures (MM$/yr.)
$\dot{B}_i$	i^{th}-effect brine mass flow rate (kg/s)
CR	compression ratio (dimensionless)

CRF	capital recovery factor (1/yr.)
$\dot{D}$	total distillate mass flow rate (kg/s)
DF	driving force (K)
$\dot{F}$	total feed mass flow rate (kg/s)
$\dot{F}_i$	i^{th}-effect feed mass flow rate (kg/s)
h_i	i^{th}-effect specific enthalpy (kJ/kg)
HTA	heat transfer area (m^2)
$\dot{L}_i$	i^{th}-effect distillate mass flow rate (kg/s)
$\dot{M}_{CW}$	cooling water mass flow rate (kg/s)
$\dot{m}_a$	air mass flow rate (kg/s)
$\dot{m}_f$	fuel mass flow rate (kg/s)
$\dot{m}_g$	combustion gas mass flow rate (kg/s)
$\dot{m}_{st}$	total mass flow rate in HRSG (kg/s)
N_E	number of distillation effects
$OPEX$	operation expenditures (MM$/yr.)
p	pressure (kPa)
$\dot{Q}$	heat/refrigeration capacity (kW)
Ra	ejector entrainment ratio (dimensionless)
$\dot{S}$	ejector discharge mixture flow rate (kg/s)
$\dot{SW}$	seawater feed mass flow rate (kg/s)
t	total operating time (6500 h/yr.)
T	temperature (K, °C)
TAC	total annual cost (MM$/yr.)
$THTA$	total heat transfer area (m^2)
U	global heat transfer coefficient ($kJ/m^2/K$)
$\dot{V}_i$	i^{th}-effect vapor mass flow rate (kg/s)
x_i	i^{th}-effect brine composition (kg/kg)
Z_k	investment cost of component k ($)

Greek symbols

α	exponential factor (dimensionless)
ΔTML	logarithm mean temperature difference (K)
λ	vaporization latent heat (kJ/kg)
η	isentropic efficiency (dimensionless)
ε	effectiveness (dimensionless)

Abbreviations

ABS	absorber
APH	air preheater
ARS	absorption refrigeration system
BPE	boiling point elevation
CC	combustion chamber
COMP	compressor
COND	condenser
DPDP	dual-purpose desalination plant

E_i	distillation effect i
ECON	economizer
EVAP	evaporator
GA	genetic algorithm
GAMS	General Algebraic Modelling System
GRG	generalized reduced gradient
GT	gas turbine
HP	high pressure
HRSG	heat recovery steam generator
HTA	heat transfer area
HTG	high-temperature generator
HTSHE	high-temperature solution heat exchanger
LP	low pressure
LTC	low-temperature condenser
LTG	low-temperature generator
LTSHE	low-temperature solution heat exchanger
MED	multi-effect distillation
MGS	multi-generation system
MSF	multiple stage flash
NGCC	natural gas combined-cycle
NLP	nonlinear programming
OF	objective function
PG	power generation
$PreH_i$	preheater i
ST	steam turbine
WH	water heater

1 Introduction

Tri-generation is the simultaneous production of electricity, heating, and refrigeration from renewable or non-renewable energy sources by integration of a power cycle with a refrigeration cycle and a heat recovery system [1]. In multi-generation systems, part of the electricity or refrigeration or heating is used to produce one or more additional products/outputs/services such as hydrogen or drying or hot water [2], or hot water and hydrogen [3, 4], or hydrogen and potable water [5, 6]. These systems constitute alternatives that help the community to satisfy global energy needs while lowering environmental impacts and costs. Reductions in fuel use, emissions of CO_2 and wastes, and improved efficiencies are potential benefits of multi-generation over single-generation [2].

In view of the variety of individual processes being integrated, scale of the integrated processes, energy prime movers, among other key aspects, tri- and multi-generation systems should be designed taking into consideration whether the extra investment for producing outputs – in addition to power – is justified in terms of revenue, payback period, levelized electricity cost, or environmental impact [1]. Thereby, different criteria should be defined to assess and compare the benefits of multi-

generation systems from multiple perspectives. Different computational, methodological, and solution approaches and tools, such as multi-objective optimization (MOO) and multivariable or simultaneous optimization techniques as well as advanced process simulation software are definitely needed. Under this perspective, two main conclusions can be drawn from a literature survey on multi-generation systems: a) although there are many works on multi-generation systems, most of them do not include a seawater desalination system in the tri- or multi-generation system [3,4,7–16], b) most of the optimization algorithms used for multi-generation systems – either with or without desalination – are of meta-heuristic type, ranging from genetic algorithms (GAs) to artificial neural networks (ANNs), as it is described next.

Applications of GAs in multi-generation systems that do not include desalination systems can be found in [17, 18] and that include distillation-based desalination systems can be found in [19–24]. A micro multi-generation system to produce power, refrigeration, heating, and freshwater has been studies in [22]. The system included a solid oxide fuel cell (SOFC), a micro gas turbine (MGT), a multi-effect distillation (MED) desalination unit, an organic steam ejector refrigerator (OSER), and a heat exchanger. The authors performed energy, exergy, economic, and environmental analyses for a reference case. Also, two MOO problems were conducted using the non-dominated sorting genetic algorithm II (NSGA-II) method, and the obtained results were compared with the reference case. The first MOO problem considered the overall energy efficiency, exergy efficiency, and total cost as objectives, while the second one considered the overall energy efficiency, freshwater production, and net power output. A result showed that the freshwater production increased by 0.1267 kg/s with respect to the reference case, while the system's overall energy efficiency decreased by 8.6%. An innovative multi-generation system using a geothermal heat source, a Kalina cycle, an absorption refrigeration system (ARS), a humidification-dehumidification (HDH) desalination system, and a domestic water heater system has been investigated in [24]. The authors employed exergoeconomic optimization and used GA. They first solved single-objective optimization (SOO) problems considering the thermal efficiency, exergy efficiency, and total cost as objective functions, and then, MOO problems considering these three objectives with different weighting coefficients.

Applications of GAs for the study of multi-generation systems based on reverse osmosis (RO) can be found in [25–27] and on MED/RO hybrid systems in [28]. The authors of [28] have evaluated a multi-generation system composed by a MED desalination unit with thermal vapor compression (TVC) and a RO desalination unit, a gas turbine (GT) unit, an absorption chiller, and parabolic trough solar collectors (PTSC) to produce power, heating, and freshwater. The authors studied the system by applying exergy, exergoeconomic, and exergoenvironmental analyses. MOO was performed to maximize the exergetic efficiency and to minimize costs and environmental impacts. To this end, multi-objective genetic algorithm (MOGA) and multi-objective water cycle algorithm

(MOWCA) were applied and compared, obtaining practically the same solutions.

Also, multi-generation systems including seawater desalination have been studied by combining GA and ANN [29, 30]. In [29] a new solar and biomass-based multi-generation system comprising a steam Rankine cycle, a double-effect ARS, a proton exchange membrane (PEM) electrolyzer, a MED desalination unit, and a PTSC has been investigated. Exergy, exergoeconomic, and exergoenvironmental analyses have been carried out to calculate the inefficiencies occurring in the components. Then, multi-criteria optimization approach based on a GA was applied to determine the optimum design of the system considering thermodynamic (exergy efficiency) and thermoeconomic (product cost) criteria. To this end, the authors used ANN to learn the relationships between inputs and outputs – black box model – from training data taken from solutions obtained by using the Engineering Equation Solver (EES). Then, the trained model was imported into the GA toolbox of MATLAB software to perform MOO aiming at the maximization of the exergy efficiency and minimization of the product cost.

The derivative-free optimization algorithms mentioned above have received considerable attention within the optimization community during the last time. They are probabilistic methods that do not need the analytical knowledge of the function. Therefore, a solution obtained from any evolutionary algorithm is better only when it is compared to other(s) solution(s), and no test is performed to check whether the "better" solution is optimal. Then, these algorithms never "know" when to stop, apart from the length of time, or the number of iterations or candidate solutions that the user wants to allow it to explore. Metaheuristic algorithms are best used on cases where it is difficult or impossible to test for optimality. However, in optimization problems where the search space has structures that can be exploited by special-purpose search techniques, GAs generally show poor efficiencies from a computational point of view. In such cases, mathematical programming techniques employing deterministic optimization algorithms are strongly suggested.

There are several articles addressing the study of multi-generation systems including desalination processes by applying exergoeconomic analysis [31–35]. Unlike other methods, exergy-based analyses provide relevant information about the exergy destruction (inefficiencies) associated to all system components through the avoidable endogenous and avoidable exogenous values and, therefore, they can be employed to design more efficient energy conversion systems [36]. However, these methods need a large number of calculations to obtain the avoidable endogenous and avoidable exogenous values and require to define both the ideal process and the so-called hybrid process, which is a subjective task having a strong influence on the obtained results.

Also, multi-generation systems including desalination have been studied by using simulation models implemented in MATLAB [37], combining HYSYS with MATLAB [38, 39], using EES

[40–42], and combining EES with TRNSYS [43, 44]. In these works, several parametric studies were conducted. In [37] was reported detailed simulations of a tri-generation system combining concentrated solar power (CSP), a steam Rankine cycle (SRC), a MED desalination unit, and an ARS to satisfy demands for 1000 residential houses. MATLAB software was used to perform the energy, exergy, and economic analyses. In [38] has been proposed an integrated system by considering an upgrading bio-LNG system, a MED desalination unit, an organic Rankine cycle (ORC), a photovoltaic system (PV), and a geothermal source, which was studied by energy and exergy analyses. HYSYS was used for simulating the LNG process and the ORC, HYSYS/MATLAB for the MED system, and PVSYST for the solar PV system. The authors showed that the integrated system can produce 5.295 kg/s of bio-LNG, 2.773 kg/s of freshwater, and 840 kW of power, with overall system's energy and exergy efficiencies of 73.2% and 76.8%, respectively. A multi-generation system to produce electricity, freshwater, hydrogen, and refrigeration by using solar and geothermal energy has been investigated in [40]. The system comprises a solar integrated ammonia fuel cell system, a RO desalination system, a PEM-based hydrogen production unit, and an ARS. One of the four used turbines works with geothermal fluid. Energy and exergy analyses were performed by using EES. The influence of the geothermal fluid and ambient temperatures, flashing pressure, and turbine efficiency on the system performance was studied parametrically. Overall energy and exergy efficiencies of 42.3% and 21.3% were obtained, respectively. In [41] the results of thermodynamic assessment of a multi-generation system to produce electrical power, refrigeration, potable and sanitary water, and hydrogen has been reported. The following subsystems were included: a SOFC unit, a GT, a biomass combustor, an ORC integrated with an ejector refrigeration system (ERS), a HDH desalination unit, and a PEM electrolyzer. A simulation model was implemented in EES to see the effect of the current density, fuel utilization factor, and SOFC inlet temperature on the generated net electrical power, refrigeration capacity, and overall energy and exergy efficiencies. The authors reported an output electrical power of 4392 kW, a refrigeration load of 164.2 kW, potable and sanitary water production rates of 41.6 m^3/d and 41.0 m^3/d, respectively, and hydrogen production rate of 67.02 kg/d, at overall energy and exergy efficiencies of 77.6% and 47.1%, respectively. Also, dynamic simulation models of multi-generation systems have been implemented in TRNSYS software package [43, 44].

Parametric-based studies using simulation models are useful to assess the performance of the examined system and to find acceptable design parameters without satisfying mathematical optimum criteria. In general, in parametric studies based on simulations, a given model parameter is varied while the other ones are kept fixed. Therefore, this approach cannot provide the optimal design parameter values of the system since the trade-offs established between all the process variables are not elucidated simultaneously. Thus, in process models where the objective function being evaluated

is influenced by several design parameters, the optimization task of such processes is not straightforward. Unlike this, the application of mathematical programming techniques performing simultaneous optimization is more convenient than the use of parametric studies based on simulations for searching for "optimal" design parameters.

Although mathematical programming is not new and it has been successfully applied to many energy conversion systems [45–52], only few articles applying simultaneous optimization of the process variables with deterministic optimization algorithms can be found in the literature, to optimize multi-generation systems including desalination processes [53–56]. For example, in [53] was developed a mixed-integer linear programming (MILP) model to study a multi-generation system to produce electrical power, refrigeration, heating, HCl, CO_2-absorbing brine, and freshwater by RO. The authors proposed a multi-period formulation to include the variations in demands of products as well as the electricity price. The resulting MILP model is a simplification of the original model since all the nonlinear constraints were linearized. The model was implemented in GAMS and solved with LINGO. HCl and CO_2-absorbing treated brine are produced in an electrolysis unit from the brine stream leaving the RO unit. Two single-objective functions based on profit and carbon footprint were formulated. A mixed-integer nonlinear programming (MINLP) model for a micro-multigeneration system capable of producing power, refrigeration, and freshwater to satisfy demands of touristic hotels in Spain was proposed in [55]. An internal combustion engine as prime mover device, a single-effect H_2O-LiBr ARS, plate heat exchangers, a small scale MED and/or RO desalination units were considered. Given the hotel location and demand specifications, the model determines the best desalination technology and the optimal capacities of the system components. The MINLP model was implemented in GAMS and solved using DICOPT.

In this paper, a nonlinear programming (NLP) model of a multi-generation energy system to produce electrical power, refrigeration, freshwater by seawater MED thermal desalination, and hot water for heating is developed and an optimization algorithm based on the generalized reduced gradient (GRG) method is used to determine the optimal number of distillation effects, sizes of the system components, and operating conditions. The studied integrated system is optimized by single-objective optimization considering two different objective functions: the total heat transfer area (THTA) and the total annual cost (TAC). Unlike published articles, the number of distillation effects in the MED process is optimized for given product specifications. To this end, and to avoid introducing discrete decisions, the optimal number of effects is determined parametrically but solving simultaneously all the trade-offs between process-unit sizes and operating conditions at the same time. Here it is worth distinguishing between parameterization of discrete decisions and parameterization of continuous decisions. In this work, the optimization problem involves only one

discrete decision – the total number of distillation effects in the MED desalination system –. If parameterization is performed on continuous decisions, then several simulations have to be executed due to the large number of combinations that should be explored, with the risk of not finding the set of optimal values for all the variables. To avoid this risk, it is proposed to optimize the continuous decisions simultaneously and vary parametrically the number of distillation effects in the MED desalination system only. It should be mentioned that the number of distillation effects can be modelled by using integer or binary variables, but this would imply a MINLP formulation type, which is more difficult to solve than a NLP formulation type. If the proposed optimization problem had involved more than one discrete decision, a MINLP formulation would have been chosen to simultaneously optimize the discrete and continuous decisions.

2 Process description

Figure 1 shows the considered multi-generation energy system for producing electrical power, freshwater, refrigeration, and heating (hot water) by integration of a power generation (PG) system, a multi-effect distillation (MED) desalination system, a series flow double-effect H_2O-LiBr absorption refrigeration system (ARS), and a water heater (WH). As shown, the PG, MED, and ARS subsystems are directly coupled through the heat recovery steam generator (HRSG), which operates at two pressure levels. The PG system basically consists of a compressor (COMP), an air preheater (APH), a combustion chamber (CC), and a gas turbine (GT). The combustion gases are expanded in the GT to generate power. A fraction of the generated power is used to run the COMP to compress the air required for combustion and the rest is provided as output electrical power. After expanded, the exhaust gases are conducted to the HRSG to produce saturated steam at two pressure levels. Each pressure level includes an economizer (ECON) and an evaporator (EVAP). The saturated high-pressure (HP) steam (S1) is sent to the first distillation effect of the MED system after passing through an ejector, where it is mixed with a fraction of the vapour generated in the last distillation effect of the MED system. After transferring its latent heat of condensation in the first effect, it is then returned back to the HP zone of the HRSG. The saturated low-pressure (LP) steam (S2) is used to power the ARS by transferring latent heat of condensation in the high-temperature generator (HTG) to vaporize the refrigerant (H_2O) from the weak LiBr solution. The condensate (saturated liquid) is passed through the water heater (WH) to provide hot water as heating output, and then, it is returned back to LP zone of the HRSG. In the ARS, the refrigerant vaporized in the HTG goes through the low-temperature generator (LTG), where it condenses transferring latent heat of condensation to the strong LiBr solution – coming from the high-temperature solution heat exchanger (HTSHE) through an expansion valve – for vaporizing an additional amount of

refrigerant. Both fractions of refrigerant are mixed and passed through the low-temperature condenser (LTC) and an expansion value to the evaporator (EVAP), where the refrigeration output is provided. The freshwater is obtained by the MED system that basically consists of in-series evaporation effects (E_i) with the corresponding preheaters ($PreH_i$), a condenser (COND), and an ejector. Freshwater (distillate) is produced by recovering the vapour of the boiling brine in the effects, which are operated at decreasing pressure levels. Since the water boiling point elevation (BPE) decreases with decreasing pressure levels, the vapour produced in one effect is used to heat the next one, except for the first (hottest) effect, which is heated by the HP steam (S1) produced in the HRSG after passing through the ejector, as mentioned.

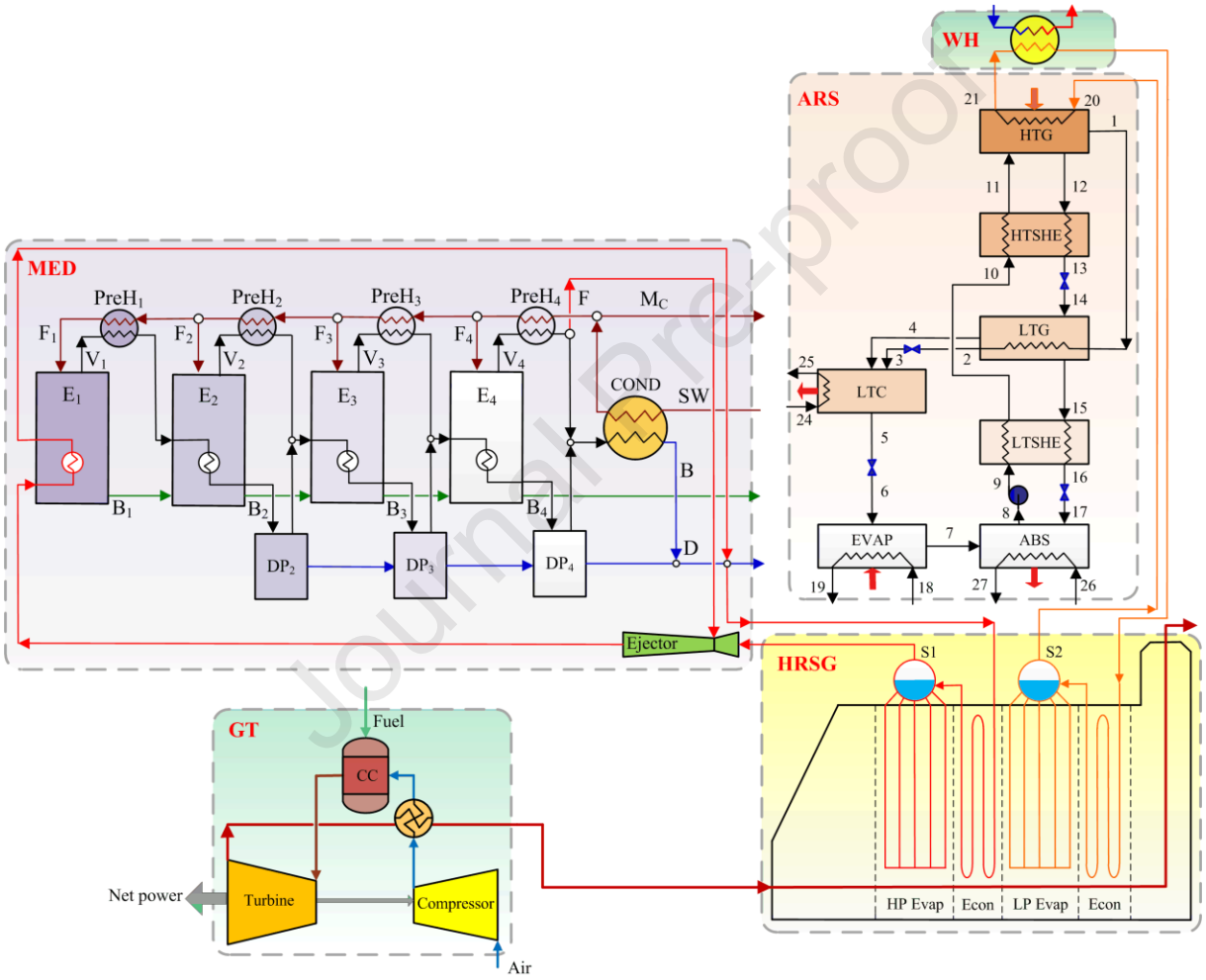

Figure 1. Multi-generation system for producing electricity, refrigeration, freshwater, and heating.

The integrated process presents several trade-offs that result from the combinations of the trade-offs associated with each subsystem. These trade-offs involve, for instance, the fuel consumption and air supply rates, flow rate, pressure, temperature, and composition values of all process streams (seawater, freshwater, strong and weak LiBr solutions, steam, cooling water), and the heat loads in the system components with their corresponding heat transfer areas and driving forces.

3 Mathematical model

A comprehensive first-principle-based mathematical model of the integrated system was derived and implemented using mathematical models of subsystems that have already been verified and validated in previous works and mathematical models developed, verified, and validated for this work. The model corresponding to the gas turbine and boiler (GT/HRSG) cycle is that used in [57] and reported elsewhere [58–60]. The model corresponding to the series flow double-effect H_2O-LiBr ARS system is that reported in [61]. Since the model of the MED system has not been previously reported, only the main model equations of this subsystem are presented. The cost model considered for the TAC minimization is also presented. The resulting mathematical model involves 583 constraints (equalities and inequalities constraints) and 570 variables. Inequalities constraints are included, for instance, to avoid temperature crosses in the heat exchangers.

3.1 Multi-effect distillation desalination system model

In a MED system, evaporation occurs in a film of seawater that is in contact with the heat transfer area. Differently, in a multiple stage flash (MSF) desalination plant, only convective heating of seawater takes place inside the tubes and the evaporation phenomenon occurs from a brine stream that flashes in each stage. Figure 2 shows a schematic of the MED system to derive the mathematical model presented next.

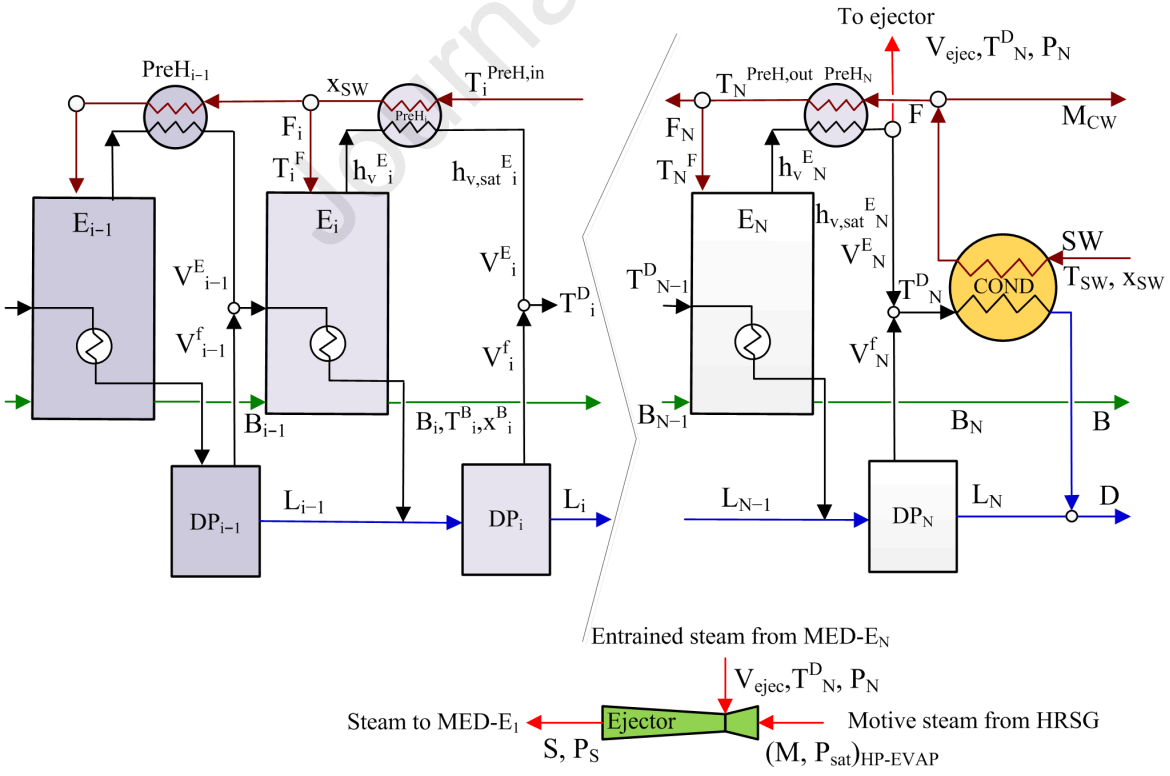

Figure 2. Schematic of the multi-effect distillation (MED) desalination system

Mass and energy balances of the distillation effect E_i:

$$\dot{F}_i = \dot{V}_i^E + \dot{B}_i \qquad i = 1 \qquad (1)$$

$$\dot{F}_i \cdot x_{SW} = \dot{B}_i \cdot x_i^B \qquad i = 1 \qquad (2)$$

$$\dot{F}_i \cdot h_i^F + \dot{S} \cdot \lambda_S = \dot{B}_i \cdot h_i^B + \dot{V}_i^E \cdot h_{V,i}^E \qquad i = 1 \qquad (3)$$

$$\dot{F}_i + \dot{B}_{i-1} = \dot{V}_i + \dot{B}_i \qquad i = 2, ..., N-1 \qquad (4)$$

$$\dot{F}_i \cdot x_{SW} + \dot{B}_{i-1} \cdot x_{i-1}^B = \dot{B}_i \cdot x_i^B \qquad i = 2, ..., N-1 \qquad (5)$$

$$\dot{F}_i \cdot h_i^F + \dot{B}_{i-1} \cdot h_{i-1}^F + (\dot{V}_{i-1}^E + \dot{V}_{i-1}^f) \cdot \lambda_{i-1} = \dot{B}_i \cdot h_i^B + \dot{V}_i^E \cdot h_{V,i}^E \qquad i = 2, ..., N-1 \qquad (6)$$

Mass and energy balances in the distillate flashing chambers DP_i:

$$\dot{V}_{i-1}^E + \dot{V}_{i-1}^f + \dot{L}_{i-1} = \dot{V}_i^f + \dot{L}_i \qquad i = 2, ..., N-1 \qquad (7)$$

$$(\dot{V}_{i-1}^E + \dot{V}_{i-1}^f + \dot{L}_{i-1}) \cdot h_{L,i-1}^f = \dot{V}_i^f \cdot h_{V,i}^f + \dot{L}_i \cdot h_{L,i}^f \qquad i = 2, ..., N-1 \qquad (8)$$

Energy balances of the pre-heater $PreH_i$ and condenser COND:

$$\dot{V}_i^E \cdot (h_{V,i}^E - h_{V,sat,i}^E) = \sum_{i' \le i} \dot{F}_i \cdot (h_i^{PreH,out} - h_i^{PreH,in}) \qquad i = 1,..., N \qquad (9)$$

$$(\dot{V}_i^E + \dot{V}_i^f) \cdot \lambda_i = \dot{SW} \cdot (h_i^{PreH,in} - h^{SW}) \qquad i = 1,..., N \qquad (10)$$

$$\dot{SW} = \dot{F} + \dot{M}_{CW} \qquad (11)$$

Heat transfer areas:

$$\dot{S} \cdot \lambda_S = U_{E,i} \cdot A_{E,i} \cdot (T_S - T_i^B) \qquad i = 1 \qquad (12)$$

$$(\dot{V}_{i-1}^E + \dot{V}_{i-1}^f) \cdot \lambda_{i-1} = U_{E,i} \cdot A_{E,i} \cdot (T_{i-1}^D - T_i^B) \qquad i = 2,..., N \qquad (13)$$

$$\dot{V}_i^E \cdot (h_{V,i}^E - h_{V,sat,i}^E) = U_{PreH,i} \cdot A_{PreH,i} \cdot DF_{PreH,i} \qquad i = 1,..., N \qquad (14)$$

$$(\dot{V}_i^E + \dot{V}_i^f) \cdot \lambda_i = U_{COND} \cdot A_{COND} \cdot DF_{COND} \qquad i = N \qquad (15)$$

where $DF_{PreH,i}$ and DF_{COND} refer to the driving forces in the preheater $PreH_i$ and condenser COND, respectively, which are calculated by the approximation in [62]; $U_{E,i}$, $U_{PreH,i}$, and U_{COND} are the overall heat transfer coefficients, which are calculated by correlations reported in [63].

Finally, the model includes the constraints associated to the steam ejector [63]:

$$Ra = 0.296 \cdot \left(\frac{P_S^{1.19}}{P_{EV}^{1.04}} \right) \cdot \left(\frac{P_M}{P_{EV}} \right)^{0.015} \left(\frac{PCF}{TCF} \right) \tag{16}$$

$$PFC = 3 \cdot 10^{-7} \cdot P_M^2 - 0.0009 \cdot P_M + 1.6101 \tag{17}$$

$$TCF = 2 \cdot 10^{-8} \cdot T_{EV}^2 - 0.0006 \cdot T_{EV} + 1.0047 \tag{18}$$

Ra is the entrainment ratio; P_M, P_S, and P_{EV} are the pressures of the motive steam (equal to $P_{sat,HP\ EVAP}$ of HRSG), discharge mixture, and entrained vapor (equal to P_N of the MED last effect *N*), respectively.

The total MED heat transfer area (HTA_{MED}) is expressed as:

$$HTA_{MED} = \sum_{i=1}^{N_E} A_{E,i} + \sum_{i=1}^{N_E} A_{PreH,i} + A_{COND} \tag{19}$$

3.2 Cost model

The total annual cost (*TAC*) used as the objective function (*OF*) is calculated taken into account the (annualized) capital expenditure (*annCAPEX*) and the operation expenditure (*OPEX*) is expressed as:

$$TAC = annCAPEX + OPEX \tag{20}$$

where *annCAPEX* is calculated by Eq. (21) in terms of the capital recovery factor (*CRF* = 0.1/yr.) and the purchased cost Z_k of each system component *k*, which is calculated by Eq. (22):

$$annCAPEX = CRF \cdot \sum_k Z_k \tag{21}$$

Cost equations reported in [64] are used to calculate the purchased cost Z_k for the heat exchangers of the ARS and MED subsystems. The factor $Z_{R,k}$ in Eq. (22) refers to the bare module factor of the component *k*, which is listed in Table 1

$$Z_k = Z_{R,k} \left(\frac{HTA_k}{HTA_{R,k}} \right)^{\alpha_k} \tag{22}$$

The factor $HTA_{R,k}$ refers to the reference size of any heat exchanger *k* – in terms of heat transfer area –. While α_k is the respective exponential factor for a component *k*. In this case, $HTA_{R,k}$ is 100 m^2 and α_k is 0.6 for the ARS components. For the MED system components, $HTA_{R,k}$ is 1 m^2 and α_k is 0.78. The cost equation to calculate the investment of the heat transfer area is taken from [65]. A cost associated with the construction/assembly of a distillation effect of the MED subsystem is also considered, which is calculated in terms of the total heat transfer area, and it is expressed as follows:

$$Z_{k,E} = Z_{R,k,E} \left(\frac{HTA_{MED}}{N_E} \right)^{\alpha_k} \tag{23}$$

Table 1. Bare module factors $Z_{R,k}$ used in Eq. (22)

ARS system [64]	Value (10^3 \$)
Generator	17.5
Condenser	8.0
Evaporator/Condenser	16.0
Absorber	16.5
Solution heat exchanger	12.0
MED system	12.0
Evaporation area [65]	9.0
Construction/assembly of an effect	12.5
APH (air pre-heater in PG system)	2.6
WH (water heating system)	8.0

The purchased costs of the components of the HRSG and PG subsystems are calculated by Eqs. (24)–(27), which are taken from [60].

$$Z_{HRSG} = \sum_j \left(Z_{HRSG,j} \left(\frac{\dot{Q}_{HRSG,j}}{\Delta TLM_{HRSG,j}} \right)^{0.8} \right) + C_{st} \cdot \dot{m}_{st} + C_g \cdot \dot{m}_g^{1.2} \tag{24}$$

where $Z_{HRSG,j}$ = 3650 \$·(kW/K)$^{0.8}$, C_{st} = 11820 \$/(kg·s), and C_g = 658 \$/(kg·s).

$$Z_{COMP} = \left(\frac{C_{11} \cdot \dot{m}_a}{C_{12} - \eta_{COMP}} \right) \cdot \left(\frac{P_2}{P_1} \right) \cdot ln\left(\frac{P_2}{P_1} \right) \tag{25}$$

where C_{11} = 39.5 \$/(kg·s) and C_{12} = 0.9.

$$Z_{CC} = \left(\frac{C_{21} \cdot \dot{m}_a}{C_{22} - \frac{P_4}{P_5}} \right) \cdot \left(1 - e^{C_{23} \cdot T_4 - C_{24}} \right) \tag{26}$$

where C_{21} = 25.6 \$/(kg·s), C_{22} = 0.995, C_{23} = 0.018/K, C_{24} = 26.4.

$$Z_{GT} = \left(\frac{C_{31} \cdot \dot{m}_g}{C_{32} - \eta_{GT}} \right) \cdot ln\left(\frac{P_4}{P_5} \right) \cdot \left(1 - e^{C_{33} \cdot T_4 - C_{34}} \right) \tag{27}$$

where C_{31} = 266.3 \$/(kg·s), C_{32} = 0.92, C_{33} = 0.036/K, and C_{34} = 54.4.

The *OPEX* accounts for the cost associated to the fuel demand and it is calculated as follows:

$$OPEX = C_S \cdot \dot{m}_f \cdot 3600 \cdot t \tag{28}$$

where C_S and t refer to the unitary cost of steam (0.006 \$/MJ) and the total operating time (6500 h/yr.), respectively.

4 Problem statement and solution strategy

4.1 Problem statement

Given the required levels of electrical power generation, freshwater production, refrigeration, and heating, the problem is to simultaneously determine the optimal operating conditions and sizes of all subsystem components that minimize (a) the total heat transfer area of the integrated multi-generation system ($THTA_{MGS}$), and (b) the total annual cost of the integrated multi-generation system (TAC). The two proposed single-objective optimization problems are formally expressed as follows (Eq. (29)):

$$\begin{aligned} &Min\ f(\boldsymbol{x}) \\ &\textit{subject to:} \\ &\begin{cases} \boldsymbol{g}(\boldsymbol{x}) = 0 \\ \boldsymbol{h}(\boldsymbol{x}) \le 0 \\ \textit{Process design specifications} \\ \textit{Process data} \\ \textit{Cost data} \\ N_E \end{cases} \end{aligned} \tag{29}$$

where $\boldsymbol{x}$ is the vector of the model optimization variables; $\boldsymbol{f(x)}$ is the objective function being minimized in each case, i.e. $\boldsymbol{f(x)}$ refers to $THTA_{MGS}$ or TAC, as appropriate; $\boldsymbol{g(x)}$ refers to the set of the equality constraints i.e. mass and energy balances, design and sizing equations, equations to calculate the physicochemical and thermodynamic properties, cost equations, among others; $\boldsymbol{h(x)}$ refers to the set of the inequality constraints, which are included, for instance, for avoiding temperature crosses between process streams in a heat exchanger. The "process design specifications" represent the model parameters associated with the required multi-generation system outputs i.e. net electrical power generation, freshwater production, and refrigeration and heating capacities. The "process data" represent the set of all type of data necessary to describe the subsystems. The symbol N_E indicates the number of distillation effects in the MED system, which is a model parameter that is parametrically varied from 4 to 6.

4.2 Optimization strategy

The optimization models and the solution strategy were implemented in the GAMS modeling environment [66]. Figure 3 shows the flowchart of the strategy proposed in this work for solving the optimization problems in GAMS environment with the generalized reduced gradient (GRG) algorithm-based CONOPT solver [67]. A pre-processing phase to initialize the model variables was included in the solution strategy to obtain an initial and feasible solution to be used in the optimization phase. As it is shown, the pre-processing phase systematically solves a sequence of simulation models of larger sizes. The strategy starts by solving 'MODEL 1', which includes the

mass and energy balances; it is solved in simulation mode as no objective function is considered. The benefit of solving this model is to obtain a feasible solution at a low computational cost; that is, to obtain values of pressures, temperatures, compositions, and flow rates that satisfy the mass and energy balances. In order to solve this simulation model, the degrees of freedom are accordingly fixed by assigning values to some model variables. For instance, some of the fixed variables are the pressure ratio in the GT and the operating pressures in the HRSG. The solution obtained for this problem is afterward used as a starting point – the initialization point – to solve 'MODEL 2', which adds to MODEL 1 the design equations to calculate the heat transfer area of all system components. In MODEL 2, the added variables associated to all driving forces and heat transfer areas are automatically initialized using the values of temperatures, enthalpies, and flow rates obtained from MODEL 1. The MODEL 2 is also a simulation model because it is solved by keeping fixed the same degrees of freedom considered in MODEL 1 and no new ones are added. Then, the solution obtained for MODEL 2 is used as the initialization point to solve 'MODEL 3', which adds to MODEL 2 the cost model equations. In MODEL 3, the added variables of the cost model are automatically initialized using the values of flow rates and sizes of the system components obtained from MODEL 2. MODEL 3 is solved keeping fixed the same degrees of freedom as in the previous models. Then, the simulation solution obtained from MODEL 3 is used to start the GRG method to optimize MODEL 3 but now including the objective function and realising the degrees of freedom i.e. previously fixed variables are now free variables. The convergence of the GRG optimization method is facilitated by the pre-processing phase since MODEL 3 – the most complex model – is optimized using an initial point that already satisfies the mass and energy balances, sizing, and cost equations. The optimal number of distillation effect N_E is obtained parametrically i.e. by applying the solution strategy – simultaneous optimization of the operating conditions, sizes, and costs of process units – for each N_E value and comparing the corresponding objective function values. Finally, it should be mentioned that the solution strategy is valid for any objective function specified by the user such as maximization of efficiencies, minimization of fuel consumption, minimization of total heat transfer area, and minimization of total cost.

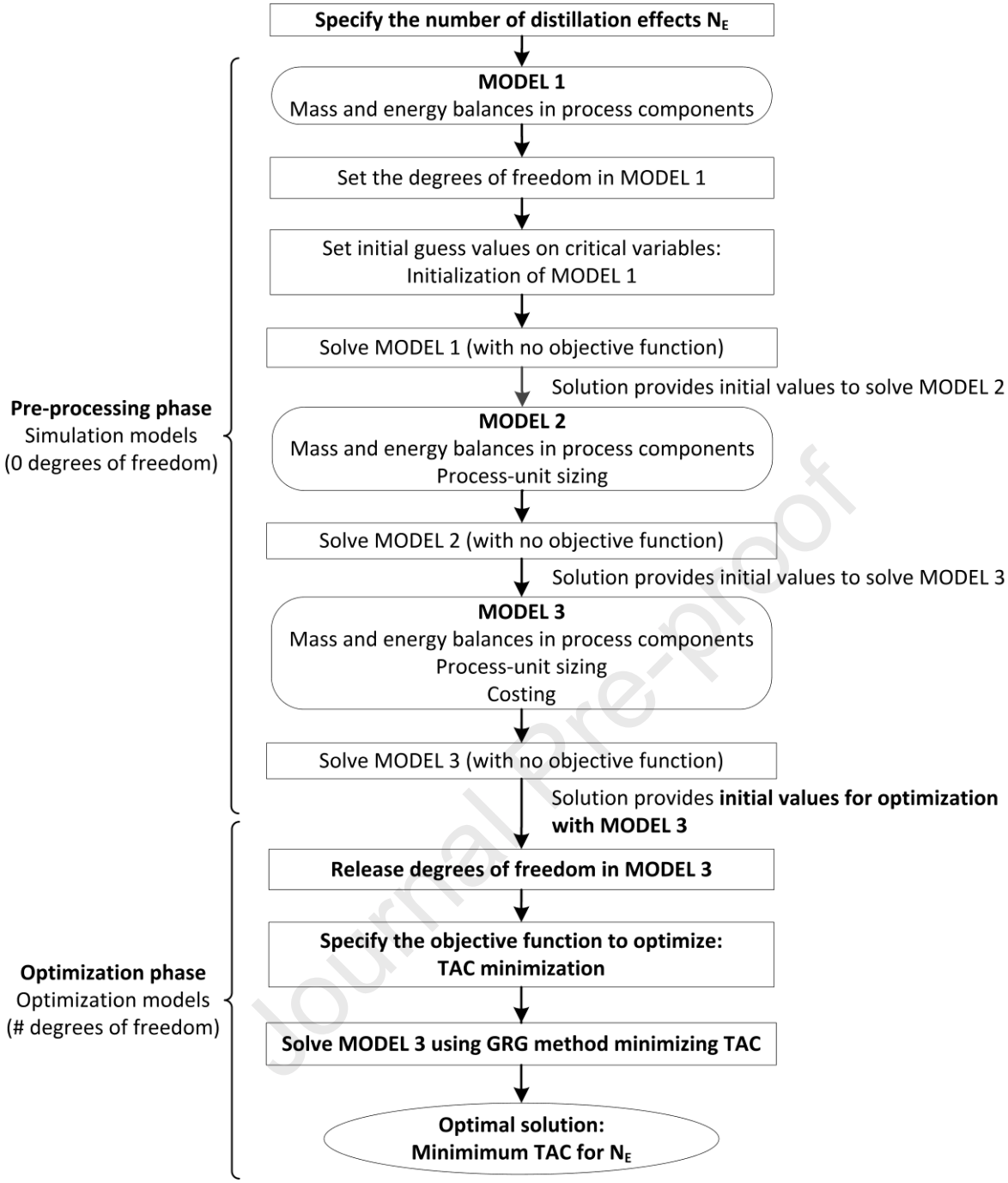

Figure 3. Flowchart of the strategy used for solving the optimization problems in GAMS with the GRG-based CONOPT code.

5 Results

Table 2 lists the considered design specifications and process data. The optimization problems formulated in Eq. (29) are solved for these values by varying parametrically the number of distillation effects (N_E) in the MED system from 4 to 6 effects. Minimization of the total heat transfer area is addressed in section 5.1 and minimization of the total annual cost in section 5.2. The main variable values obtained for the three numbers of distillation effects are presented and compared in

Tables 3–10 and Figures 4–9.

Table 2. Process design specifications and data

Process design specifications	Value
Net electrical power generation (kW)	36971
Freshwater production (kg/s)	100
Refrigeration capacity (kW)	2000
Evaporator temperature (ºC)	6.0
Heating water (kW)	745
Process data	
Seawater temperature (ºC)	25.0
Seawater salinity (ppm)	30000
Fuel temperature (ºC)	25.0
Fuel lower heating value (kJ/kg)	50000
Air composition (mole fraction)	79% N_2, 21% O_2
Cooling water temperature (ºC)	25.0

5.1 Minimization of the total heat transfer area of the integrated system

The results in Table 3 indicate that the minimum total area of the multi-generation system ($THTA_{MGS}$) required for 4 effects is 39148 m^2, of which 26283 m^2 correspond to the MED subsystem and 11319.8 m^2 to the PG/HRSG subsystem. The ARS and WH subsystems require only 1543.5 m^2 and 2.140 m^2, respectively.

Table 3. Minimal $THTA_{MGS}$ and optimal areas for different N_E values

	Area, *HTA* (m^2)		
Systems	4 effects	5 effects	6 effects
Integrated system ($THTA_{MGS}$)	39148	36002	35161
Subsystems			
MED	26283	24103	23874
PG	1431.5	1431.5	1431.5
HRSG	9888.3	8922.3	8310.3
ARS	1543.5	1543.5	1543.5
WH	2.140	2.140	2.140

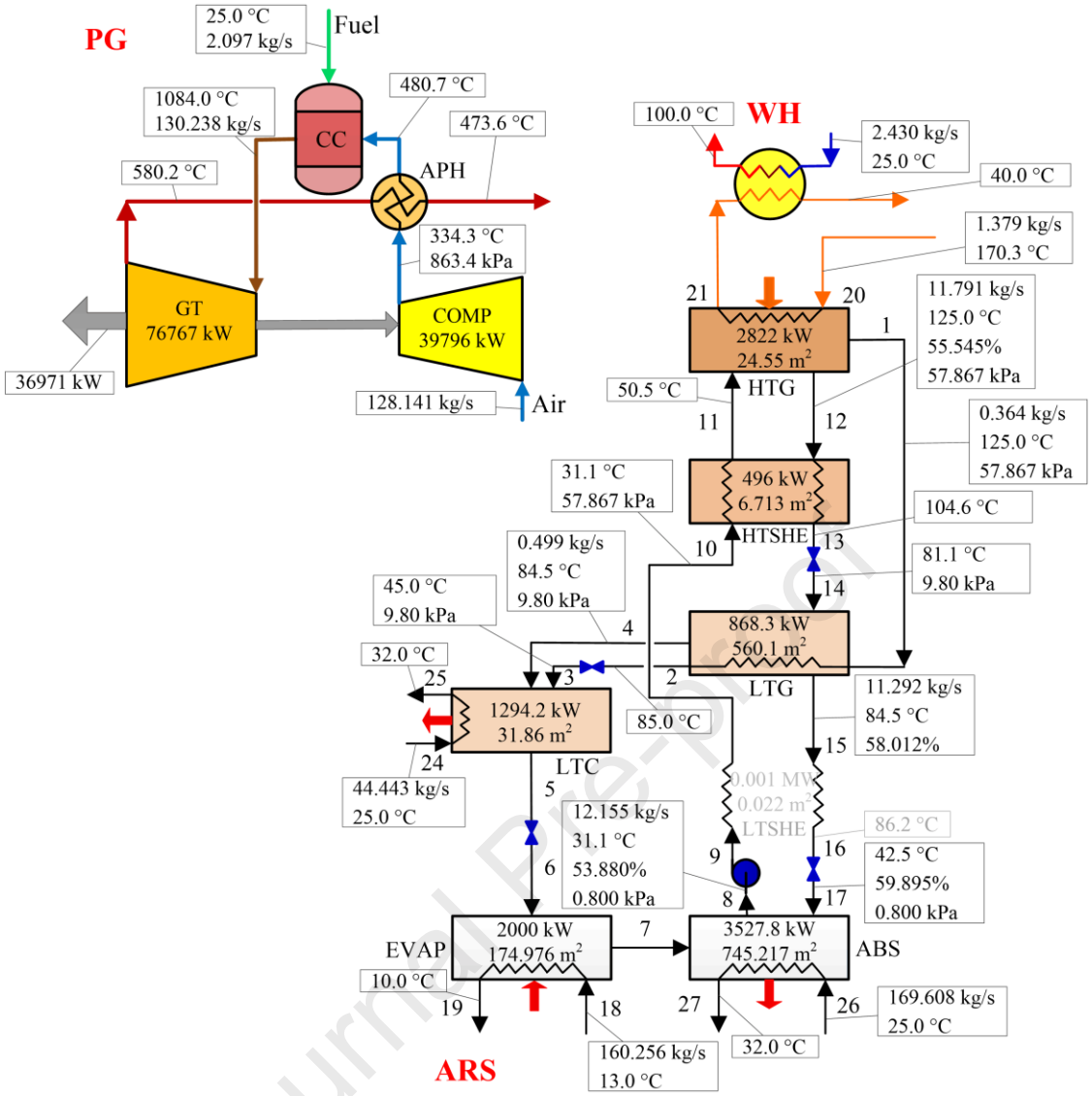

Figure 4. Optimal solution obtained for the PG, ARS, and WH subsystems by $THTA_{MGS}$ minimization

It can be seen in Table 3 that the addition of a fifth distillation effect reduces the $THTA_{MGS}$ value by around 8.0% with respect to a four-effect MED system (36002 m^2 vs. 39148 m^2) as a consequence of a reduction in the HTA_{MED} by 8.3% (24103 m^2 vs. 26283 m^2) and in the HTA_{HRSG} by 9.8% (8922.3 m^2 vs. 9888.3 m^2). No variation in the HTA_{PG}, HTA_{ARS}, and HTA_{WH} values is observed. The optimal values of all the decision variables corresponding to the PG, ARS, and WH systems are shown in Figure 4, which are the same for the three analyzed cases (N_E = 4, 5, 6). Figure 5 and Table 4 report the optimal area, heat load, and driving force values in the MED desalination effects, preheaters, and condenser for different N_E values.

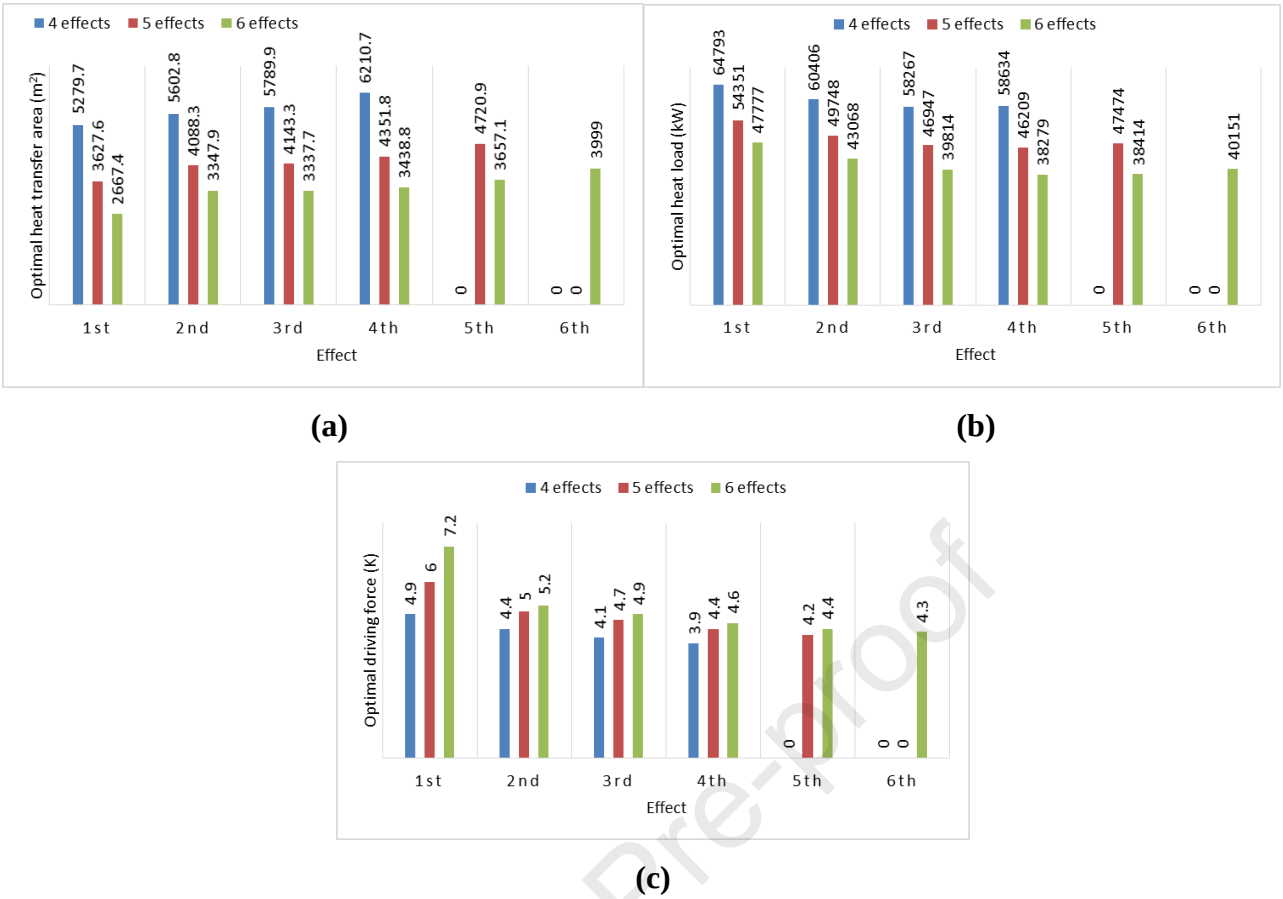

Figure 5. $THTA_{MGS}$ minimization. (a) Optimal area, (b) heat load, and (c) driving force values for different N_E values

According to Table 5, compared to a four-effect MED system, one main advantage of adding a fifth effect is that the last one operates at a lower temperature (47.2 ºC vs. 54.4 ºC) leading to a more convenient profile of temperature between the first and last distillation effects, resulting in a lower heating steam demand in the first effect (23.429 kg/s vs. 27.897 kg/s) and, consequently, a lower associated area (3627.6 m^2 vs. 5279.7 m^2, Fig. 5).

Table 4. Optimal area, heat load, and driving force values in MED preheaters and condenser for different N_E values (see individual effects E_i in Fig. 5)

	N_E		
MED components	4	5	6
– Preheaters			
Total heat load, $Q_{T,PreH}$ (kW)	3658.9	3857.3	4009.0
Total area, $THTA_{PreH}$ (m^2)	19.83	16.59	14.30
– Condenser			
Heat load, Q_{COND} (kW)	35931	33440	34039
Area, HTA_{COND} (m^2)	3379.9	3154.2	3411.3
Driving force, DF_{COND} (K)	9.5	8.5	7.4

Table 5. Optimal values of mass flow rate, pressure, and temperature of main streams and total heat recovered in HRSG for different N_E values

Systems	N_E		
	4	5	6
– HRSG			
Total recovered heat (kW)	44407	43590	43121
Gas inlet temperature (ºC)	473.6	473.6	473.6
Gas outlet temperature (ºC)	182.2	187.6	190.6
– ARS			
LP-level steam to HTG			
Mass flow rate (kg/s)	1.379	1.379	1.379
Pressure (kPa)	800.0	800.0	800.0
– Steam ejector			
Ejector CR	2.625	3.937	5.881
Motive steam (from HRSG)			
Mass flow rate (kg/s)	16.500	16.217	16.096
Pressure (kPa)	1340.4	1248.5	1080.2
Entrained steam (from MED last effect)			
Mass flow rate (kg/s)	11.397	7.212	4.525
Pressure (kPa)	14.64	10.21	7.18
– MED system			
Feed flow rate to each effect (kg/s)	69.903	51.247	40.499
Steam entering first effect (from ejector)			
Mass flow rate (kg/s)	27.897	23.429	20.621
Pressure (kPa)	38.43	40.22	42.23
Temperature (ºC)	74.9	76.0	77.2
Brine temperature (ºC)			
First effect (E_1)	70.0	70.0	70.0
Last effect	54.4	47.2	40.5

This lower heating steam requirement can be achieved in several ways, in which the ejector plays a key role. One possibility is to extract less amount of steam from the HRSG without significantly varying its pressure maintaining the amount of entrained vapor in the ejector. Another possibility is to maintain a similar heating steam flow rate and extraction pressure in the HRSG and extract less amount of vapor from the last effect. In this case, the best possibility is one that allows reducing the HTA_{HRSG} value. According to Table 5, the heating steam extracted from the HRSG for 5 effects is slightly lesser than that extracted for 4 effects (16.217 kg/s vs. 16.500 kg/s) but at a lower pressure (1248.5 kPa vs. 1340.4 kPa), while the entrained vapor flow rate entering the ejector decreases from 11.397 kg/s to 7.212 kg/s and the vapor compression ratio increases from 2.625 to 3.937. According to Fig. 6, these reductions not only allow the heat loads in the HP-EVAP and HP-ECON to decrease with respect to 4 effects (32163 kW vs. 32532 kW in HP-EVAP, and 7843.6 kW vs. 8290.8 kW in HP-ECON) but also to increase the driving forces (154.5 °C vs. 148.6 °C in HP-EVAP, and 100.8 °C vs. 95.5 °C in HP-ECON), both variations positively affecting the reduction in the areas of both components (4624.8 m^2 vs. 4865.3 m^2 in HP-EVAP, and 1946.1 m^2 vs. 2171.3 m^2 in HP-ECON). Since the heat load required in the first effect of the 5-effect system is lesser than that

required in the 4-effect system, the heat to be recovered in the HRSG is lesser (43590 kW vs. 44407 kW) and the temperature of the gases leaving the HRSG is 5.3 ºC higher (187.6 ºC vs. 182.2 ºC) due to the conditions at the GT exit are the same for all cases. As mentioned above, the optimal variable values obtained for the PG, ARS, and WH subsystems are the same for the three N_E values (Figure 4). Regarding the PG subsystem, the generation of 36971 kW for any number of MED effects N_E requires 128.088 kg/s and 2.150 kg/s of air and fuel, respectively, and 1431.5 m^2 in the air preheater APH to transfer 16268 kW with a driving force of 113.6 ºC. For all N_E values, the heat available in the HRSG is the same since the hot gas flow rate and temperature entering the HRSG are the same (130.238 kg/s and 473.6 ºC, respectively) but the heat recovered depends on the heating steam requirement in the MED first effect, which in turn depends on the number of effects. The greater the number of effects, the less amount of heat and area requirements in the MED system, resulting in less heat recovered in the HRSG and, consequently, less HRSG area. Despite the fact that the objective function consists in minimizing the $THTA_{MGS}$, the solution allocates 1431.5 m^2 in the APH of the PG system to achieve the optimal flow rate and temperature values of the hot gases entering the HRSG to produce the steam required in the other subsystems. However, these optimal values depend only on the power generation (results not shown) but not on the number of MED effects since the greatest reduction in the area is achieved in the HRSG – by modifying the temperature of the gases and the conditions of the generated steam – as well as in the MED subsystem itself – by modifying the flow rate, pressure, and temperature of the seawater, distillate, and brine streams –. Regarding the ARS, its behaviour is similar to that observed for the PG subsystem in that the optimal variable values of this subsystem (heat loads, areas, and driving forces) are the same for all numbers of distillation effects (Figure 4).

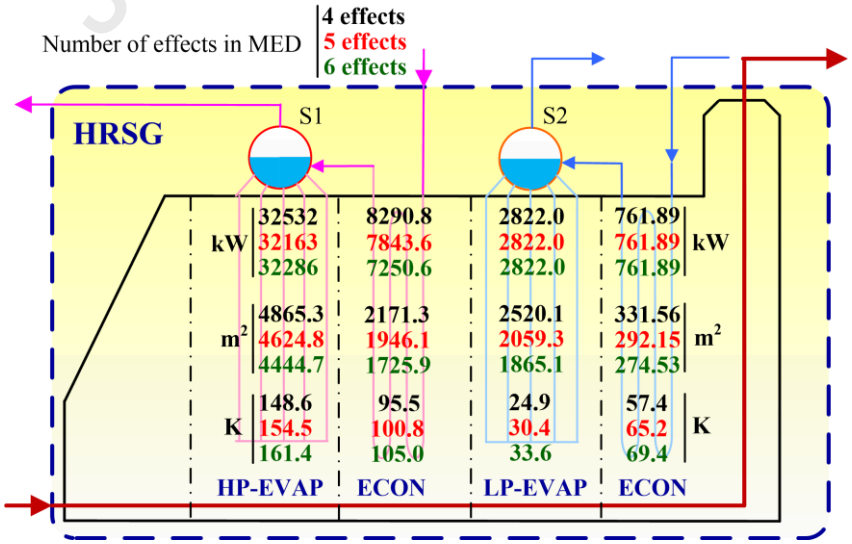

Figure 6. Area, heat load, and driving force values in the HRSG system for different N_E values

According to Figure 4, in the ARS, the HTG heat load is 2822.0 kW, which is satisfied by the steam generated in the LP-EVAP in the HRSG coldest zone (Figure 1). The LP-steam closed circuit connected to the ARS is physically independent of the HP-steam closed circuit connected to the MED system. However, the temperature of the gases that heat the LP closed circuit depend on the temperature of the gases that heat the HP closed circuit, which vary with the number of MED effects. For this reason, although the heat loads in the LP-EVAP and LP-ECON are the same for any number of effects, the areas are different due to the variation of the driving forces, which depend on the gas temperature. For example, according to Fig. 6, the heat load in the LP-EVAP is 2822.0 kW in all cases, while the LP-EVAP area required for 4 effects is by around 22.4% larger than that for 5 effects and the LP-EVAP driving force is by around 18.1% lower. Interestingly, the optimal ARS configuration includes the HTSHE but eliminates the LTSHE, as shown in Figure 4 (in gray color). From the energy integration point of view, it would not be convenient, a priori, to eliminate the LTSHE since it would require increasing the heating utility demand in the HTG. Since the $THTA_{MGS}$ minimization is considered in this first case study, the optimal trade-off between the required energy and the associated areas indicates that, in order to reduce the objective function value, it is preferable to eliminate the LTSHE (at the cost of an increase in the HTG area as a consequence of a slight increase in the HTG heat load) and maintain the HTSHE with an area of 6.713 m^2 – to exchange 496.48 kW with an associated driving force of 73.9 K –. In case that the HTSHE is also eliminated (by forcing to zero its effectiveness ε_{HTSHE}), the increase in the HTG area would directly increase the $THTA_{MGS}$ value.

Analyzing the values in Tables 3–5 and Figs.4–6, it can be concluded that the variable behaviours obtained by adding a sixth distillation effect to a 5-effect MED system are qualitatively the same but with an impact on the area values significantly smaller than those obtained by adding a fifth effect to a 4-effect system. The presented results show that the addition of a distillation effect does not imply an increase in the $THTA_{MGS}$ but, on the contrary, it implies a decrease in it, since the heat loads, areas, and driving forces are distributed more conveniently throughout the effects. This can be clearly seen when comparing the distributions of these variables for the three values of number of effects studied. This tendency can be confirmed if a seventh effect is added to a 6-effect system i.e. the $THTA_{MGS}$ is reduced but the percentage decrease is not significant (results not shown). In that case, the pressure level of the steam generated in the HRSG to power the MED system decreases, tending to the pressure level of the steam generated for the ARS. Then, the HRSG heat exchanger configuration may change and even lead to the unification of the two steam circuits – the two pressure levels – thus requiring only one economizer-evaporator pair.

5.2 Minimization of the total annual cost of the integrated system

Maintaining the same design specifications as in the previous case, it is proposed to simultaneously determine the optimal process-unit dimensions and operating conditions that minimize the total annual cost (*TAC*) of the integrated system by varying parametrically the number of distillation effects (N_E).

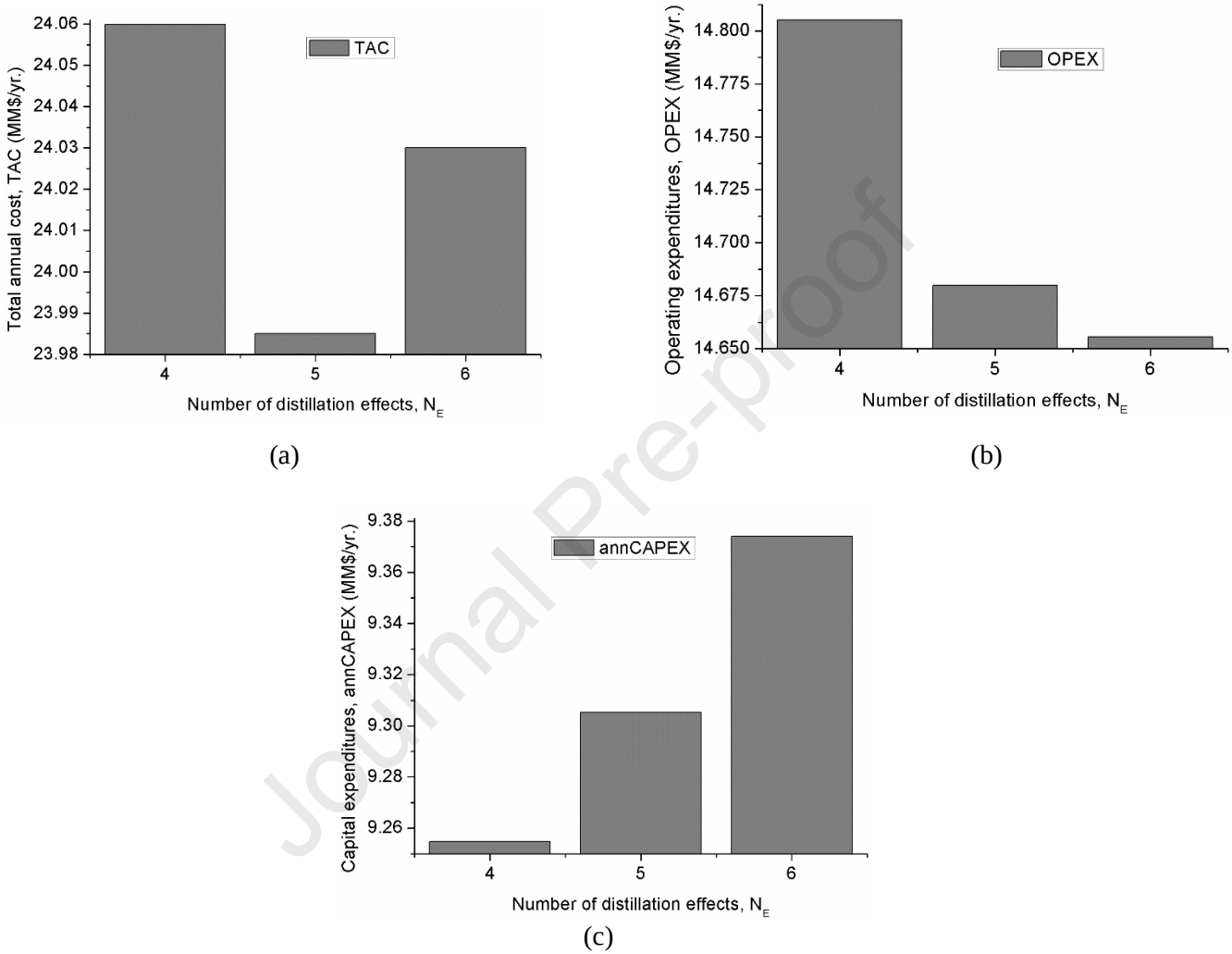

Figure 7. *TAC* minimization. a) Minimal *TAC*, b) optimal *OPEX*, c) optimal *annCAPEX*.

Figure 7 compares the minimum *TAC* values and the corresponding optimal *OPEX* and *annCAPEX* values obtained for 4, 5, and 6 effects. Tables 6–10 compare the cost distribution, operating conditions of the main process streams, and areas, heat loads and driving forces of the main process units.

Table 6. *TAC* minimization. *TAC*, *OPEX*, and *annCAPEX* values, and contributions of the process units to the total investment.

	N_E		
	4	5	6
***TAC* (MM$/yr.)** [a]	**24.060**	**23.985**	**24.030**
***OPEX* (MM$/yr.)**	**14.805**	**14.680**	**14.656**
***annCAPEX* (MM$/yr.)**	**9.255**	**9.305**	**9.374**
Z_{TOTAL} **(MM$)**	**92.547**	**93.054**	**93.741**
Z_{MED} **(MM$)**	**87.485**	**87.967**	**88.645**
Cost for area of pre-heaters, effects and condenser [b]	43.925	43.088	42.532
Construction/assembly cost of effects [c]	43.560	44.879	46.113
Z_{PG} **(M$)**	**3773.29**	**3597.4**	**3606.6**
Z_{GT}	1705.6	1480.5	1480.6
Z_{COMP}	1171.5	839.10	838.98
Z_{APH}	767.21	1154.9	1164.0
Z_{CC}	128.98	122.90	122.95
Z_{HRSG} **(M$)** [d]	**1152.7**	**1347.8**	**1347.6**
$Z_{HP\text{-}EVAP}$	245.98	275.81	276.81
$Z_{HP\text{-}ECON}$	136.00	144.69	143.70
$Z_{LP\text{-}EVAP}$	316.97	447.32	447.32
$Z_{LP\text{-}ECON}$	47.68	61.84	61.84
Z_{ARS} **($)**	**136090**	**140820**	**140820**
Z_{HTG}	7445	7691	7691
Z_{ABS}	55680	55062	55062
Z_{LTG}	44135	49209	49209
Z_{HTSHE}	2373	2373	2373
Z_{EVAP}	22382	22382	22382
Z_{COND}	3998	4027	4027
Z_{LTSHE}	76	78	78
Z_{WH} **($)**	**786**	**796**	**796**

(a) 1 M$ refers to 1×10^3 $; 1 MM$ refers to 1×10^6 $.
(b) Cost associated to the total heat transfer area required by pre-heaters, effects, and condenser.
(c) Cost associated with the construction/assembly of the distillation effects.
(d) Z_{HRSG} includes the 5th and 6th terms present in Eq. (24).

According to Fig. 7a and Table 6, it is observed that the obtained minimum *TAC* value is 23.985 MM$/yr. and that it corresponds to a MED system having 5 distillation effects. The *TAC* values are similar as the difference between the values corresponding to 5 and 4 effects is only −0.075 MM$/yr. (23.985 MM$/yr. vs. 24.060 MM$/yr.) and those corresponding to 6 and 5 effects is +0.045 MM$/yr. (24.030 MM$/yr. vs. 23.985 MM$/yr.). This is due to the equilibrium point between *OPEX* and *annCAPEX*. Table 6 and Figs. 7b and 7c show that an increase in the number of distillation effects produces a decrease in OPEX (Fig. 7b), which is practically of the same magnitude as the increase in *annCAPEX* (Fig. 5c), thus resulting in no significant variations in *TAC*. However, the relative variations between the reduction in *OPEX* and the increase in *annCAPEX* for increasing N_E values determine a minimum *TAC* value and, consequently, an optimal N_E value. When N_E increases from 4 to 5 distillation effects, *OPEX* decreases 0.125 MM$/yr. while

annCAPEX increases 0.050 MM$/yr., thus resulting in a reduction in *TAC* of 0.075 MM$/yr., as mentioned. When N_E increases from 5 to 6 distillation effects, *OPEX* decreases only by 0.024 MM$/yr. due to a decrease in fuel consumption of 0.018 kg/s (Table 7) while the *annCAPEX* increases by 0.069 MM$/yr., thus resulting in an increase in *TAC* of 0.045 MM$/yr., as mentioned. In other words, when N_E increases from 4 to 5 effects the decrease in *OPEX* is more important than the increase in *annCAPEX*, contrary to what happens when N_E increases from 5 to 6 effects.

Table 7. *TAC* minimization. Optimal mass flow rate, pressure, and temperature values of main streams and total heat recovered in HRSG for different N_E values.

	N_E		
Systems	4	5	6
– PG			
Compressor CR	6.558	5.125	5.124
Fuel (kg/s)	2.109	2.091	2.088
Air (kg/s)	115.222	125.259	125.263
Inlet temperature at the combustor chamber (K)	783.9	846.6	848.0
– HRSG			
Gases exhaust (kg/s)	117.331	127.350	127.350
Gas inlet temperature (K)	781.6	737.7	736.5
Gas outlet temperature (K)	439.8	437.2	437.2
– ARS			
LP-level steam to HTG			
Mass flow rate (kg/s)	1.348	1.374	1.374
Pressure (kPa)	800.0	755.0	755.0
– Steam ejector			
Ejector CR	2.932	4.261	6.665
Motive steam (from HRSG)			
Mass flow rate (kg/s)	17.549	16.686	16.667
Pressure (kPa)	1446.5	1433.2	1410.6
Entrained steam (from MED last effect)			
Mass flow rate (kg/s)	10.822	6.924	4.291
Pressure (kPa)	13.50	9.65	6.59
– MED system			
Feed flow rate to each effect (kg/s)	71.333	50.354	40.119
Steam entering first effect (from ejector)			
Mass flow rate (kg/s)	28.371	23.792	20.958
Pressure (kPa)	39.57	41.13	43.95
Temperature (ºC)	75.6	76.5	78.1
Brine temperature (ºC)			
First effect (E_1)	70.0	70.0	70.0
Last effect	52.7	46.1	38.9

Regarding the influence of the PG subsystem on the *annCAPEX* value, it can be observed that when N_E increases from 4 to 5 distillation effects, the fuel consumption decreases (Table 7) due to an increase in the area of the air preheater (HTA_{PG}) of 951.8 m^2 (from 1539.6 m^2 to 2491.4 m^2, Table 8), consequently increasing the cost Z_{APH} associated with this area (from 0.767 MM$ to 1.155 MM$, Table 6). This increase in the APH heat transfer area (HTA_{PG}) determines an increase in the air

temperature at the combustor inlet of 62.7 K (from 783.9 K to 846.6 K, Table 7), and it also allows the compressor COMP to operate at a lower compression ratio *CR* (5.125 vs. 6.558, Table 7), reducing its investment cost Z_{COMP} from 1.171 MM$ to 0.839 MM$ (Table 6). The decrease in the fuel flow rate is accompanied by a decrease in the air flow rate, which implies a reduction in the investment required for the combustor Z_{CC} from 0.129 MM$ to 0.123 MM$. Thus, it is observed that it is convenient to increase the HTA_{PG} since it allows to consume less fuel (and consequently to reduce the *OPEX* value) and to reduce the investment required for the compressor and combustor.

Regarding the influence of the MED system on the *annCAPEX* value, it can be observed in Table 6 that the investment required by this subsystem Z_{MED} increases with increasing N_E values despite the fact that its total area decreases (Table 8). As observed in Table 6, the part of the investment cost that is directly associated with the area decreases with increasing N_E values but the part of the investment cost associated with the construction/assembly of the effects – calculated based on the area (Eq. 23) – increases with increasing N_E values. Consequently, the convenience of including or not an additional distillation effect depends on the relative variations of the decrease and increase of both components of the investment cost Z_{MED}. In this case, the 5-effect system is the one that determines the optimal cost variations that lead to the minimum *TAC* value of the integrated system.

Table 8. *TAC* minimization. Optimal area distribution for different N_E values

Systems	Area, *HTA* (m^2)		
	4 effects	5 effects	6 effects
Integrated system ($THTA_{MGS}$)	43016	46982	46630
Subsystems			
MED	23512	22947	22568
PG	1539.6	2491.4	2516.9
HRSG	16499	19997	19999
ARS	1463.3	1544.4	1544.4
WH	2.092	2.136	2.136

Regarding the influence of the HRSG subsystem on the *annCAPEX* value, the investment Z_{HRSG} increases when N_E increases from 4 to 5 effects due to the increase in the total area required by the four heat exchangers (Figure 9) and gas flow rate. When N_E increases from 5 to 6 effects the investment Z_{HRSG} remains practically constant (Table 6) due to mainly the variations of the HTA of the HP-EVAP – which increases 26.4 m^2 – and of the HP-ECON – which decreases 24.5 m^2 – resulting in a net increase of only 1.9 m^2 (Figure 9). Slight variations in the gas and steam flow rates are observed in Table 7, mainly between the 4-effect system and the rest.

(a) **(b)**

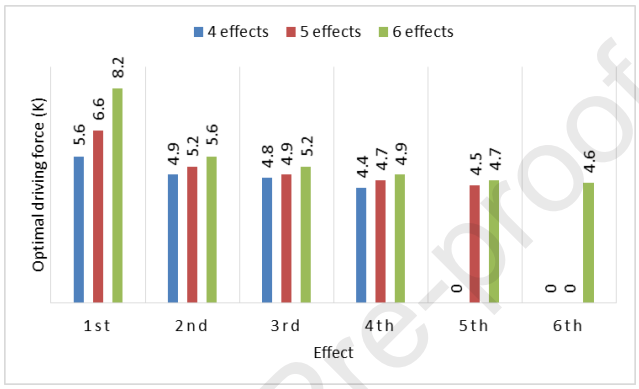

(c)

Figure 8. *TAC* minimization. (a) Optimal area, (b) heat load, and (c) driving force values in the MED system for different N_E values.

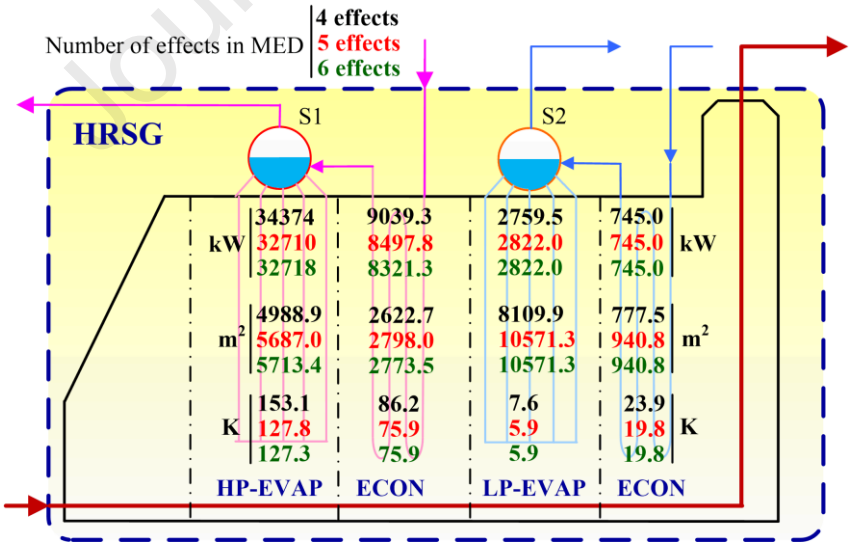

Figure 9. *TAC* minimization. Optimal area, heat load, and driving force values in the HRSG system for different N_E values

The influence of the ARS subsystem on the *annCAPEX* value is similar for the three N_E values. It is one order of magnitude lesser than those of the PG and HRSG subsystems and 2 orders of magnitude lesser than that of the MED subsystem (Table 6).

The distribution of the minimal $THTA_{MGS}$ is shown in Table 8, where it is observed that the increase in HTA_{HRSG} and HTA_{PG} of the 5-effect system with respect to the 4-effect one is more important than the decrease in HTA_{MED}, resulting in an increase in $THTA_{MGS}$ of 3966 m^2 (46982 m^2 vs. 43016 m^2). On the contrary, the decrease in HTA_{MED} of the 6-effect system with respect to the 5-effect one is more important than the increase in HTA_{HRSG} and HTA_{PG}, resulting in a decrease in $THTA_{MGS}$ of 352 m^2 (46630 m^2 vs. 46982 m^2). The decrease in HTA_{MED} is also influenced by the optimal conditions obtained for the steam entering the first effect (flow rate and pressure), which depend in turn on the HRSG and ejector operation conditions. It is observed in Table 7 that the steam flow rate required in the first effect decreases with increasing N_E values, but the pressure increases slightly. The decrease in the steam flow rate entering the first effect is due to the optimal operating conditions of the ejector, preferring to extract less amount of steam from the last effect and generate practically the same amount of steam in the HRSG but at lower pressure values, which causes an increase in the HTA_{HRSG} due to mainly the increase in the $HTA_{LP\text{-}EVAP}$ (from 8109.9 m^2 to 10571.3 m^2, Figure 9). The compression ratio *CR* in the ejector increases with increasing N_E values because the entrained steam is at lower temperatures. For instance, for N_E = 4 the CR value is 2.932 and the entrained steam temperature is 52.7 °C, while for N_E = 6 the *CR* value is 6.665 and the entrained steam temperature is 38.9 °C (Table 7).

Table 9 reports the optimal area, heat load, and driving force values in the preheaters and condenser of the MED desalination system for different N_E values.

Table 9: *TAC* minimization. Optimal area, heat load, and driving force values in MED preheaters and condenser for different N_E values

	N_E		
MED components	4	5	6
– Preheaters			
Total heat load, $Q_{T,PreH}$ (kW)	3574	3913	4047
Total area, $THTA_{PreH}$ (m^2)	16.54	15.73	13.12
– Condenser			
Heat load, Q_{COND} (kW)	37705	34184	34644
Area, HTA_{COND}, (m^2)	3307.2	3134.16	3377.97
Driving force, DF_{COND} (K)	9.9	8.6	7.5

Table 10 presents the optimal values obtained for the ARS. It can be observed that this subsystem does not show significant variations in the operating conditions and areas of its components, except for the LTG. The HTA_{ARS} increases slightly from 1463.3 m^2 to 1544.4 m^2 when N_E increases from 4 to 5. This behavior is associated with the behavior of the LP steam generated by

the LP-EVAP and LP-ECON in the HRSG. No variations are observed when N_E increases from 5 to 6 because the pinch temperature values are reached in most heat exchangers of the ARS. The LTSHE area value obtained for the three N_E values (0.022 m^2) is comparatively negligible with respect to those obtained for the other components since its effectiveness ε_{LTSHE} reaches the imposed lower bound (0.1%), thus indicating that the inclusion of LTSHE is not beneficial in this case.

Table 10. *TAC* minimization. Optimal area, heat load, and driving force values obtained for ARS for different N_E values

	Area (m^2)			Heat load (kW)			Driving force (K)		
N_E	4	5	6	4	5	6	4	5	6
HTG	24.046	25.406	25.406	2759.5	2822.0	2822.0	76.5	74.0	74.0
LTG	466.64	560.20	560.20	884.60	868.30	868.30	1.223	1.000	1.000
LTSHE	0.022	0.022	0.022*	1.197	1.243	1.243	55.520	55.223	55.223
HTSHE	6.713	6.713	6.713	493.84	496.48	496.48	73.563	73.956	73.956
COND	31.469	31.860	31.860	1278.3	1294.2	1294.2	16.249	16.249	16.249
ABS	759.44	745.22	745.22	3481.1	3527.8	3527.8	6.548	6.763	6.763
EVAP	174.98	174.98	174.98	2000.0	2000.0	2000.0	7.620	7.620	7.620
Total	1463.3	1544.4	1544.4						

(*) Value reached the lower bound.

6 Conclusions

This paper focused on the optimization of a multi-generation system by integrating a dual-purpose desalination plant (DPDP) and a low-scale absorption refrigeration system (ARS). The DPDP consisted of a gas turbine (GT) cycle to produce electricity, a heat recovery steam generator (HRSG) operating with two closed steam cycles coupled with a multi-effect distillation (MED) desalination plant – to produce freshwater – and a double-effect series flow H_2O-LiBr ARS – for refrigeration –. Also, a water heater (WH) for recovering energy from the ARS heating stream was included for heating purpose.

For this study, a nonlinear mathematical programming (NLP) optimization model was derived. Mass and energy balances and equations for design and sizing of the system components as well as a cost model were included. Given process design specifications (36971 kW of electrical power generation, 100 kg/s of freshwater production, 2000 kW of refrigeration capacity, and 761.9 kW of thermal load for heating supplied by hot water), the integrated system was optimized for different numbers of distillation effects in the MED system (4–6 effects) by minimizing two objective functions by single-objective optimization: the total heat transfer area ($THTA_{MGS}$) and the total annual cost (*TAC*).

For four distillation effects, the minimum $THTA_{MGS}$ required was 39148 m^2, of which 67.1%

corresponded to the MED subsystem and 28.9% to the PG and HRSG subsystems together. For five effects, the minimal $THTA_{MGS}$ value was significantly reduced by 8.0% with respect to the obtained for the 4-effect MED system, maintaining similar percentage distribution among the subsystems. For six distillation effects, the $THTA_{MGS}$ value was reduced by 2.3% with respect to the 5-effect system. For the examined numbers of distillation effects, the obtained area values of the electricity generation system HTA_{PG} (more precisely, of the air pre-heater HTA_{APH}) and those of all ARS components were the same. In addition, it was observed that, in all cases, the optimal solution did not include the low-temperature solution heat exchanger (LTSHE) of the ARS but selected the solution heat exchanger operating at the high-temperature zone (HTSHE).

However, interestingly, an optimal number of distillation effects in the MED system was found when *TAC* was minimized. Maintaining the same process design specifications as in the previous case, the obtained minimum *TAC* value is 23.985 MM$/yr. The optimization results show that when N_E increases from 4 to 5 distillation effects the decrease in *OPEX* is more important than the increase in *annCAPEX*, contrary to what happens when N_E increases from 5 to 6 distillation effects, thus leading to an optimal value of the number of effects in the desalination system. The relative variations between the reduction in *OPEX* and the increase in *annCAPEX* for increasing N_E values determine a minimum *TAC* value and, consequently, an optimal N_E value. When N_E increases from 4 to 5 distillation effects, *OPEX* decreases 0.125 MM$/yr. while *annCAPEX* increases 0.050 MM$/yr., thus resulting in a reduction in *TAC* of 0.075 MM$/yr., as mentioned. When N_E increases from 5 to 6 distillation effects, *OPEX* decreases only by 0.024 MM$/yr. due to a decrease in fuel consumption of 0.018 kg/s while the *annCAPEX* increases by 0.069 MM$/yr., thus resulting in an increase in *TAC* of 0.045 MM$/yr., as mentioned.

From the Process System Engineering perspective, this work contributes with a mathematical optimization model for the optimal design and operation of multi-generation energy systems of similar nature to the investigated in this study. The model is able to optimize any desired design specifications as well as different objective functions such as the minimization of the total annual cost, total heat transfer area, or fuel consumption.

References

[1] Dincer I, Zamfirescu C. Chapter 9 - Multigeneration Systems, Editor(s): Dincer I., Zamfirescu C.: Advanced Power Generation Systems. Elsevier, 2014, PP. 517-573, ISBN 9780123838605.

[2] Dincer I, Rosen MA. Cogeneration, Multigeneration, and Integrated Energy Systems. Exergy Analysis of Heating, Refrigerating and Air Conditioning, 2015.

[3] Ahmadi P., Dincer I., Rosen M A. Development and assessment of an integrated biomass-based multi-generation energy system. Energy 2013; 56:155–166.

https://doi.org/10.1016/j.energy.2013.04.024

[4] Ahmadi P, Dincer I, Rosen MA. Thermodynamic modeling and multi-objective evolutionary-based optimization of a new multigeneration energy system. Energy Conversion and Management 2013; 76: 282–300. https://doi.org/10.1016/j.enconman.2013.07.049

[5] Alirahmi SM, Rostami M, Farajollahi AH. Multi-criteria design optimization and thermodynamic analysis of a novel multi-generation energy system for hydrogen, cooling, heating, power, and freshwater. International Journal of Hydrogen Energy 2020; 45(30): 15047-15062. https://doi.org/10.1016/j.ijhydene.2020.03.235

[6] Ehyaei MA, Baloochzadeh S, Ahmadi A, Abanades S. Energy, exergy, economic, exergoenvironmental, and environmental analyses of a multigeneration system to produce electricity, cooling, potable water, hydrogen and sodium-hypochlorite. Desalination Volume 2021; 501: 114902. https://doi.org/10.1016/j.desal.2020.114902

[7] Khaliq A, Choudhary K, Dincer I. Exergy analysis of a gas turbine trigeneration system using the Brayton refrigeration cycle for inlet air cooling. Proceedings of IMechE, Part A: Journal of Power and Energy 2010; 224: 449–461. https://doi.org/10.1243/09576509JPE897

[8] Ahmadi P, Rosen MA, Dincer I. Greenhouse gas emission and exergo-environmental analyses of a trigeneration energy system. Int. J. of Greenhouse Gas Control 2011; 5: 1540–1549. https://doi.org/10.1016/j.ijggc.2011.08.011

[9] Al-Sulaiman FA, Dincer I, Hamdullahpur F. Energy analysis of a trigeneration plant based on solid oxide fuel cell and organic Rankine cycle. International Journal of Hydrogen Energy 2010; 35: 5104–5113. https://doi.org/10.1016/j.ijhydene.2009.09.047

[10] Sadeghi M, Chitsaz A, Mahmoudi SMS, Rosen MA. Thermoeconomic optimization using an evolutionary algorithm of a trigeneration system driven by a solid oxide fuel cell. Energy 2015; 89: 191–204. https://doi.org/10.1016/j.energy.2015.07.067

[11] Yao E, Wang H, Wang L, Xi G, Maréchal F. Thermo-economic optimization of a combined cooling, heating and power system based on small-scale compressed air energy storage. Energy Conversion and Management 2016; 118: 377–386. https://doi.org/10.1016/j.enconman.2016.03.087

[12] Dincer I, Bicer Y. Chapter 4 - Integration of conventional energy systems for multigeneration, Ed(s): Dincer I., Bicer Y., Integrated Energy Systems for Multigeneration, Elsevier, 2020, pp. 143-221. ISBN 9780128099438.

[13] DinAli M, Dincer I. Development and analysis of an integrated gas turbine system with compressed air energy storage for load leveling and energy management. Energy 2018; 163: 604–617. https://doi.org/10.1016/j.energy.2018.08.094

[14] Al-Zareer M, Dincer I, Rosen MA. Modeling and performance assessment of a new integrated gasification combined cycle with a water gas shift membrane reactor for hydrogen production. Computers & Chemical Engineering 2017; 103: 275–292. https://doi.org/10.1016/j.compchemeng.2016.11.024

[15] Bicer Y, Dincer I. Energy and exergy analyses of an integrated underground coal gasification with SOFC fuel cell system for multigeneration including hydrogen production. International Journal of Hydrogen Energy 2015; 40: 13323–13337. https://doi.org/10.1016/j.ijhydene.2015.08.023

[16] Bicer Y, Dincer I. Development of a multigeneration system with underground coal gasification integrated to bitumen extraction applications for oil sands. Energy Conversion and Management 2015; 106: 235–248. https://doi.org/10.1016/j.enconman.2015.09.020

[17] Ahmadi P, Dincer I, Rosen MA. Thermoeconomic multi-objective optimization of a novel biomass-based integrated energy system. Energy, 2014; 68: 958-970. https://doi.org/10.1016/j.energy.2014.01.085

[18] Boyaghchi FA, Molaie H. Advanced exergy and environmental analyses and multi objective optimization of a real combined cycle power plant with supplementary firing using evolutionary algorithm. Energy 2015; 93: 2267-2279. https://doi.org/10.1016/j.energy.2015.10.094

[19] Sani MM, Noorpoor A, Motlagh M. Optimal model development of energy hub to supply water, heating and electrical demands of a cement factory. Energy 2019; 177: 574-592. https://doi.org/10.1016/j.energy.2019.03.043

[20] Beyrami J, Chitsaz A, Parham K, Arild Ø. Optimum performance of a single effect desalination unit integrated with a SOFC system by multi-objective thermo-economic optimization based on genetic algorithm. Energy 2019; 186: 115811. https://doi.org/10.1016/j.energy.2019.07.141

[21] Ansari K, Sayyaadi H, Amidpour M. Thermoeconomic optimization of a hybrid pressurized water reactor (PWR) power plant coupled to a multi effect distillation desalination system with thermo-vapor compressor (MED-TVC). Energy 2010; 35(5): 1981-1996. https://doi.org/10.1016/j.energy.2010.01.013

[22] You H, Han J, Liu Y, Chen C, Ge Y. 4E analysis and multi-objective optimization of a micro poly-generation system based on SOFC/MGT/MED and organic steam ejector refrigerator. Energy 2020; 206: 118122. https://doi.org/10.1016/j.energy.2020.118122

[23] Ghasemi A, Heidarnejad P, Noorpoor A. A novel solar-biomass based multi-generation energy system including water desalination and liquefaction of natural gas system: Thermodynamic and thermoeconomic optimization. Journal of Cleaner Production 2018; 196: 424-437. https://doi.org/10.1016/j.jclepro.2018.05.160

[24] Ghaebi H, Namin AS, Rostamzadeh H. Performance assessment and optimization of a novel multi-generation system from thermodynamic and thermoeconomic viewpoints. Energy Conversion and Management 2018; 165: 419-439. https://doi.org/10.1016/j.enconman.2018.03.055

[25] Chitgar N; Moghimi M. Design and evaluation of a novel multi-generation system based on SOFC-GT for electricity, fresh water and hydrogen production. Energy 2020; 197: 117162. https://doi.org/10.1016/j.energy.2020.117162

[26] Eveloy V, Rodgers P, Alili AA. Energy Multi-objective optimization of a pressurized solid oxide fuel cell–gas turbine hybrid system integrated with seawater reverse osmosis. Energy 2017; 123: 594-614. https://doi.org/10.1016/j.energy.2017.01.127

[27] Esfahani IJ, Yoo CK. Exergy analysis and parametric optimization of three power and fresh water cogeneration systems using refrigeration chillers. Energy 2013; 59: 340-355. https://doi.org/10.1016/j.energy.2013.07.040

[28] Vazini Modabber H, Khoshgoftar Manesh M.H. Optimal exergetic, exergoeconomic and exergoenvironmental design of polygeneration system based on gas Turbine-Absorption Chiller-Solar parabolic trough collector units integrated with multi-effect desalination-thermal vapor compressor-reverse osmosis. Renew. Energy 2021; 165: 533–552. https://doi.org/10.1016/j.renene.2020.11.001

[29] Hashemian N, Noorpoor A. Assessment and multi-criteria optimization of a solar and biomass-based multi-generation system: Thermodynamic, exergoeconomic and exergoenvironmental aspects. Energy Conversion and Management 195 (2019) 788–79. https://doi.org/10.1016/j.enconman.2019.05.039

[30] Nazari N, Porkhial S. Multi-objective optimization and exergo-economic assessment of a solar-biomass multi-generation system based on externally-fired gas turbine, steam and organic Rankine cycle, absorption chiller and multi-effect desalination. Applied Thermal Engineering 2020; 179: 115521. https://doi.org/10.1016/j.applthermaleng.2020.115521

[31] Makkeh SA, Ahmadi A, Esmaeilion F, Ehyaei MA. Energy, exergy and exergoeconomic optimization of a cogeneration system integrated with parabolic trough collector-wind turbine with desalination. Journal of Cleaner Production 2020; 273: 123122. https://doi.org/10.1016/j.jclepro.2020.123122

[32] Mohammed RH, Ibrahim MM, Abu-Heiba A. Exergoeconomic and multi-objective optimization analyses of an organic Rankine cycle integrated with multi-effect desalination for electricity, cooling, heating power. Energy Conversion and Management 2021; 231: 113826. https://doi.org/10.1016/j.enconman.2021.113826

[33] Calise F, Dentice d'Accadia M, Piacentino A. Energy Exergetic and exergoeconomic analysis of a renewable polygeneration system and viability study for small isolated communities. Energy 2015; 92(3): 290-307. https://doi.org/10.1016/j.energy.2015.03.056

[34] Calise F, Denticed'Accadia M, Macaluso A, Piacentino A, Vanoli L. Exergetic and exergoeconomic analysis of a novel hybrid solar–geothermal polygeneration system producing energy and water. Energy Conversion and Management 2016; 115: 200-220. https://doi.org/10.1016/j.enconman.2016.02.029

[35] Zhou S, Liu X, Bian Y, Shen S. Energy, exergy and exergoeconomic analysis of a combined cooling, desalination and power system. Energy Conversion and Management 2020; 218: 113006. https://doi.org/10.1016/j.enconman.2020.113006

[36] Morosuk T, Tsatsaronis G. Strengths and Limitations of Advanced Exergetic Analyses. ASME 2013 International Mechanical Engineering Congress and Exposition, San Diego, California, USA Paper No: IMECE2013-64320, V06BT07A026. https://doi.org/10.1115/IMECE2013-64320

[37] Abdelhay AO; Fath HES; Nada SA. Solar driven polygeneration system for power, desalination and cooling. Energy 2020; 198: 117341. https://doi.org/10.1016/j.energy.2020.117341

[38] Ghorbani B, Ebrahimi A, Moradi M, Ziabasharhagh M. Energy, exergy and sensitivity analyses of a novel hybrid structure for generation of Bio-Liquefied natural Gas, desalinated water and power using solar photovoltaic and geothermal source. Energy Convers. Manag. 2020; 222: 113215. https://doi.org/10.1016/j.enconman.2020.113215

[39] Ghorbani B, Miansari M, Zendehboudi S, Hamedi MH. Exergetic and economic evaluation of carbon dioxide liquefaction process in a hybridized system of water desalination, power generation, and liquefied natural gas regasification. Energy Convers. Manag. 2020; 205: 112374. https://doi.org/10.1016/j.enconman.2019.112374

[40] Siddiqui O, Dincer I. A new solar and geothermal based integrated ammonia fuel cell system for multigeneration. International Journal of Hydrogen Energy 2020; 45(60): 34637-34653. https://doi.org/10.1016/j.ijhydene.2020.02.109

[41] Haghghi MA, Holagh SG, Chitsaza A, Parham K. Thermodynamic assessment of a novel multi-generation solid oxide fuel cell-based system for production of electrical power, cooling, fresh water, and hydrogen. Energy Conversion and Management 2019; (197): 111895. https://doi.org/10.1016/j.enconman.2019.111895

[42] Anvari S, Mahian O, Taghavifar H, Wongwises S, Desideri U. 4E analysis of a modified multigeneration system designed for power, heating/cooling, and water desalination. Applied Energy 2020; 270: 115107. https://doi.org/10.1016/j.apenergy.2020.115107

[43] Calise F, Macaluso A, Piacentino A, Vanoli L. A novel hybrid polygeneration system supplying

energy and desalinated water by renewable sources in Pantelleria Island. Energy 2017; 137: 1086-1106. https://doi.org/10.1016/j.energy.2017.03.165

[44] Calise F, Dentice d'Accadia M, Vanoli R, Vicidomini M. Transient analysis of solar polygeneration systems including seawater desalination: A comparison between linear Fresnel and evacuated solar collectors. Energy 2019; 172: 647-660. https://doi.org/10.1016/j.energy.2019.02.001

[45] Mores PL, Manassaldi JI, Scenna NJ, Caballero JA, Mussati MC, Mussati SF. Optimization of the design, operating conditions, and coupling configuration of combined cycle power plants and CO2 capture processes by minimizing the mitigation cost. *Chemical Engineering Journal 2018;* 331: 870-894. https://doi.org/10.1016/j.cej.2017.08.111

[46] Piacentino A, Gallea R, Cardona F, Lo Brano V, Ciulla G, Catrini P. Optimization of trigeneration systems by Mathematical Programming: Influence of plant scheme and boundary conditions. Energy Conversion and Management 2015; 104: 100–114. https://doi.org/10.1016/j.enconman.2015.03.082

[47] Fuentes-Cortés LF, Dowling AW, Rubio-Maya C, Zavala VM, Ponce-Ortega JM. Integrated design and control of multigeneration systems for building complexes. Energy 2016; 116(P2): 1403-1416. https://doi.org/10.1016/j.energy.2016.05.093

[48] Liu P, Pistikopoulos EN. A Multi-Objective Optimization Approach to Polygeneration Energy Systems Design. AIChE J 2010; 56(5): 1218–1234. https://doi.org/10.1002/aic.12058

[49] Mazzei MS, Mussati MC, Mussati SF.NLP model-based optimal design of LiBr-H2O absorption refrigeration systems. *International Journal of Refrigeration* 2014; 38: 58-70. https://doi.org/10.1016/j.ijrefrig.2013.10.012

[50] Rubio-Maya C, Uche-Marcuello J, Martínez-Gracia A, Bayod-Rújula AA. Design optimization of a polygeneration plant fuelled by natural gas and renewable energy sources. Appl. Energy 2011; 88(2): 449–457. https://doi.org/10.1016/j.apenergy.2010.07.009

[51] Oliva DG, Francesconi JA, Mussati MC, Aguirre PA. Modeling, synthesis and optimization of heat exchanger networks. Application to fuel processing systems for PEM fuel cells. International Journal of Hydrogen Energy 2011; 36(15): 9098 – 9114. https://doi.org/10.1016/j.ijhydene.2011.04.097

[52] Mussati SF, Aguirre PA, Scenna NJ. Optimization of alternative structures of integrated power and desalination plants. Desalination 2005; 182(1-3): 123-1291. https://doi.org/10.1016/j.desal.2005.03.012

[53] Tan RR, Aviso KB, Foo DCY, Lee JY, Ubando AT. Optimal synthesis of negative emissions polygeneration systems with desalination. Energy 2019; 187: 115953.

https://doi.org/10.1016/j.energy.2019.115953

[54] Belmonte BA, Benjamin MFD, Tan RR. Optimization-based decision support methodology for the synthesis of negative-emissions biochar systems. Sustainable Production and Consumption 2019; 19: 105-116. https://doi.org/10.1016/j.spc.2019.03.008

[55] Rubio-Maya C, Uche J, Martínez A. Polygeneration plants to supply energy and desalted water in hotels located at the Spanish coast. Desalination and Water Treatment 2009; 7(1-3): 132-141. https://doi.org/10.5004/dwt.2009.716

[56] Rubio-Maya C, Uche J, Martínez A. Sequential optimization of a polygeneration plant. Energy Conversion and Management 2011; 52(8-9): 2861–2869. https://doi.org/10.1016/j.enconman.2011.01.023

[57] Mussati S. Optimal synthesis and design of dual purpose desalination plants. PhD Thesis, 2003, Universidad Nacional del Litoral, Argentina.

[58] Nemati A, Nami H, Ranjbar F, Yari M. A comparative thermodynamic analysis of ORC and Kalina cycles for waste heat recovery: A case study for CGAM cogeneration system, Case Studies in Thermal Engineering 2017; 9: 1–13. https://doi.org/10.1016/j.csite.2016.11.003

[59] Soltani R, Mohammadzadeh Keleshtery P, Vahdati M, Khoshgoftar Manesh MH, Rosen MA, Amidpour M. Multi-objective optimization of a solar-hybrid cogeneration cycle: Application to CGAM problem. Energy Conversion and Management 2014; 81: 60–71. https://doi.org/10.1016/j.enconman.2014.02.013

[60] Tsatsaronis G, Pisa J. Exergoeconomic evaluation and optimization of energy systems — application to the CGAM problem. Energy 1994; 19: 287–321.
https://doi.org/10.1016/0360-5442(94)90113-9

[61] Mussati SF, Cignitti S, Mansouri SS, Gernaey KV, Morosuk T, Mussati MC. Configuration optimization of series flow double-effect water-lithium bromide absorption refrigeration systems by cost minimization. Energy Conversion and Management 2018; 158: 359–372. https://doi.org/10.1016/j.enconman.2017.12.079

[62] Chen JJJ. Comments on improvements on a replacement for the logarithmic mean. Chemical Engineering Science 1987; 42: 2488–2489. https://doi.org/10.1016/0009-2509(87)80128-8

[63] El-Dessouky H.T., Ettouney H.M.: Fundamentals of Salt Water Desalination, Elsevier, 2002. ISBN: 0-444-50810-4.

[64] Jing Y, Li Z, Liu L, Lu S. Exergoeconomic Assessment of Solar Absorption and Absorption-Compression Hybrid Refrigeration in Building Cooling. Entropy 2018; 20(130): 1–22. https://doi.org/10.3390/e20020130.

[65] Al-hotmani OMA, Al-Obaidi MA, Patel R, Mujtaba IM. Performance analysis of a hybrid system of multi effect distillation and permeate reprocessing reverse osmosis processes for

seawater desalination. Desalination 2019; 470: 114066.
https://doi.org/10.1016/j.desal.2019.07.006

[66] GAMS Development Corporation, General Algebraic Modeling System (GAMS) Release 23.6.5. Washington, DC, USA: 2010.

[67] Drud A. CONOPT 3 solver manual. Bagsvaerd, Denmark: ARKI Consulting and Development A/S; 2012.

Highlights

A multi-generation system is integrated for power, freshwater, cooling, and heating

NLP model for simultaneous optimization is proposed and gradient-based method is used

The total heat transfer area (THTA) of the entire process is minimized

The total annual cost (TAC) of the entire process is minimized

A minimum TAC of 23.9 MM$/yr. is found when five-effect MED desalination unit is used

Declaration of interests

X The authors declare that they have no known competing financial interests or personal relationships that could have appeared to influence the work reported in this paper.

☐The authors declare the following financial interests/personal relationships which may be considered as potential competing interests: